Persistent deep-water formation in the Nordic Seas during Marine Isotope Stages 5 and 4 notwithstanding changes in Atlantic overturning

Tim B. Stobbe[1*], Henning A. Bauch[2,3], Daniel A. Frick[1], Jimin Yu[4,5], Julia Gottschalk[1]

[1]Institute of Geosciences, Kiel University, Kiel, Germany; [2]GEOMAR Helmholtz Centre for Ocean Research, Kiel, Germany; [3]Alfred Wegener Institute Helmholtz Centre for Polar and Marine Research, Bremerhaven, Germany; [4]Laoshan Laboratory, Qingdao, China; [5]Research School of Earth Sciences, Australian National University, Canberra, Australia

Correspondence to: Tim B. Stobbe (tim.stobbe@ifg.uni-kiel.de)

Short Summary: New bottom water reconstructions in the deep Norwegian Sea show higher [CO_3^{2-}] values in Marine Isotope Stages 5 and 4 than in the Holocene. This suggests modern-like/persistent deep-water formation in this region, even when Atlantic overturning weakened and/or shoaled. Our data puts new constraints on the endmember [CO_3^{2-}] composition of northern component waters emerging from the Nordic Seas, with implications for the chemical characteristics and carbon storage capacity of the Atlantic Ocean.

Keyword group 1: Nordic Seas, Carbonate ion, Atlantic Ocean, AMOC, last glacial cycle, epibenthic foraminiferal B/Ca

Key word group 2: Carbon cycle, Glacial CO_2 storage, deep-water formation, late Pleistocene, benthic foraminifera

Abstract. Alongside shifts in Pacific- and Southern Ocean carbon cycling, reductions in the extent and formation of North Atlantic Deep Water (NADW) and the expansion of southern sourced waters in the Atlantic Ocean were linked to enhanced marine carbon storage during glacial periods and are considered key mechanisms explaining late Pleistocene atmospheric CO_2 variations on glacial-interglacial timescales. However, changes in the formation of deep waters in the Nordic Seas, an important source of NADW, and their influence on the geometry and intensity of Atlantic overturning remain poorly understood, especially beyond the last glacial maximum, leaving possible impacts on atmospheric CO_2 changes elusive. Here, we present high-resolution *Cibicidoides wuellerstorfi* B/Ca-based bottom water [CO_3^{2-}] reconstructions, alongside with complementary *C. wuellerstorfi* stable oxygen and carbon isotopes and abundance estimates of aragonitic pteropods in marine sediment core PS1243 from the deep Norwegian Sea to investigate past deep-water dynamics in the Nordic Seas and potential impacts on Atlantic overturning and carbon cycling. Our data suggest continuous formation of dense and well-ventilated (high-[CO_3^{2-}]) deep waters throughout Marine Isotope Stages (MIS) 5 and 4, alongside a deepening of the aragonite compensation depth by at least 700 m between MIS 5b and MIS 4 (91–57 ka before present), consistent with sustained Nordic Seas convection. In addition, slightly higher, yet statistically significant mean bottom water [CO_3^{2-}] during MIS 5e (*sensu stricto*, 126–116 ka before present) compared to the Holocene (last 10 ka) highlight the resilience of Nordic Seas overturning towards a warmer North Atlantic, decreased Arctic sea ice extent and meltwater supply from surrounding ice sheets, although centennial-scale perturbations cannot be excluded. A compilation of bottom water [CO_3^{2-}] records from the Atlantic Ocean indicates that dense waters from the Nordic Seas may have continuously expanded into the intermediate and/or deep (western) North Atlantic via supply of dense water overflows across the Greenland-Scotland Ridge, diminishing the capacity of the North Atlantic to store

carbon during MIS 4. Our study emphasises differences in the sensitivity of North Atlantic and Nordic Seas overturning dynamics to climate boundary conditions of the last glacial cycle that have implications for the carbon storage capacity of the Atlantic Ocean and its role in atmospheric CO_2 variations.

1 Introduction

The Atlantic Meridional Overturning circulation (AMOC) is crucial for the moisture- and heat supply to the high northern latitudes, thus affecting both global climate and regional weather patterns (e.g., Rahmstorf, 2002; Adkins, 2013). Heat and moisture released by the northward flowing North Atlantic Current and the inflow of Atlantic waters into the subpolar Nordic Seas referred to as Nordic heat pump may affect northern-hemisphere ice sheet growth (e.g., Fettweis et al., 2017; Hermann et al., 2020) and leads to mild winters in western Europe at present-day (e.g., Johns et al., 2011). Inflowing saline surface waters of Atlantic origin cool and lose buoyancy within the Nordic Seas, and along with contributions of Arctic waters, sink as denser water masses to depths of up to 2 km (Mauritzen, 1996; Marshall and Schott, 1999). As an important 'gateway' between the North Atlantic and the Arctic Ocean, the Nordic Seas are therefore one of only few regions globally characterised by open-ocean convection and deep-water formation, with dense overflow waters leaving the Nordic Seas and constituting the main source of North Atlantic Deep Water (NADW; e.g., Quadfasel and Käse, 2007; Østerhus et al., 2019).

Changes in the Atlantic overturning geometry and strength were suggested to influence the carbon sequestration efficiency in the Atlantic Ocean, with impacts on atmospheric CO_2 ($CO_{2,atm}$) levels (e.g., Yu et al., 2016, 2023; Gottschalk et al., 2019). At present-day, the Nordic Seas are considered a sink for anthropogenic CO_2 due to high surface-water CO_2 uptake and deep-water transport, promoted by strong winds, vigorous primary productivity, and deep convection (Sabine et al., 2004; Rysgaard et al., 2009; Watson et al., 2009). During past glacial periods, particularly the last glacial maximum (LGM), overturning in the Nordic Seas was argued to have either weakened (e.g., Yu et al., 2008; Ezat et al., 2014, 2017a, 2021), nearly ceased (e.g., Boyle and Keigwin, 1987; Sarnthein et al., 1994; Rahmstorf, 2002; Thornalley et al., 2015) or remained similar to modern-like conditions (Hoffmann et al., 2013; Oppo et al., 2018; Larkin et al., 2022). However, most of the recent evidence supports active dense water formation in the Nordic Seas during the LGM (e.g., Ezat et al., 2021; Larkin et al., 2022). In the Atlantic Ocean, NADW is generally believed to have shoaled to above ~2.5 km water depth during the LGM forming Glacial North Atlantic Intermediate Water (GNAIW) (e.g., McManus et al., 2004; Curry and Oppo, 2005; Yu et al., 2008; Muglia and Schmittner, 2021). Bottom water carbonate ion ($[CO_3^{2-}]$) reconstructions in the Atlantic Ocean have shown that this glacial shift in Atlantic water mass geometry was characterised by shoaled GNAIW with high bottom water $[CO_3^{2-}]$ and the expansion of nutrient-rich Antarctic Bottom Water (AABW) with lower bottom water $[CO_3^{2-}]$ (Yu et al., 2008, 2010a,b, 2014; Raitzsch et al., 2011; Broecker et al., 2015; Gottschalk et al., 2015; Crocker et al., 2016; Lacerra et al., 2017; Chalk et al., 2019; Kirby et al., 2020; Yu et al., 2023). These changes were further accompanied by shifts in the dynamics of Antarctic Intermediate Water (Lacerra et al., 2019; Oppo et al., 2023). The North Atlantic Ocean was also suggested to be influenced by the outflow of high-$[CO_3^{2-}]$ Nordic Seas-sourced waters (NSSW) into the North Atlantic during the LGM, suggested to have occurred at

water depths above 2.8 km (Yu et al., 2008, Crocker et al., 2016; Ezat et al., 2021), though contributions to abyssal North Atlantic waters remain debated (Keigwin and Swift, 2017; Ezat et al., 2019; Larkin et al., 2022). Yet, the interplay of Nordic Seas convection and Atlantic overturning via dense overflow water supply and its influence on Atlantic Ocean carbon storage across various timescales remains poorly known.

One geological time interval that serves as an ideal testbed to study the circulation- and carbon cycling dynamics in the Nordic Seas and its impact on the Atlantic Ocean is the climatic optimum of the last interglacial period, i.e. Marine Isotope Stage (MIS) 5e (130–116 ka before present, BP). MIS 5e is often considered to provide crucial insights into climate system processes and feedback mechanisms under future climate conditions (e.g., Fischer et al., 2018; Guarino et al., 2020), because temperatures in the northern hemisphere were several °C warmer than today as a result of a strong, orbitally induced maximum in boreal summer insolation (e.g., NGRIP Members, 2004; Clark and Huybers, 2009; Past Interglacials Working Group of PAGES, 2016). However, although this is confirmed by sea surface temperature (SST) reconstructions from the North Atlantic (e.g., Bauch et al., 2012; Rodrigues et al., 2017), reconstructed SSTs in the Nordic Seas were lower than today (e.g., Cortijo et al., 1994; Bauch et al., 1999). In addition, albeit $CO_{2,atm}$ concentrations were at pre-industrial levels during MIS 5e (Bereiter et al., 2015), the Arctic Ocean was found to be (nearly) ice-free during MIS 5e summers (Otto-Bliesner et al., 2006; Guarino et al., 2020). Therefore, fresh water forcing induced by higher Arctic summer insolation during MIS 5e (CAPE Last Interglacial Project Members, 2006) might have also affected ocean salinities in the Nordic Seas, and hence deep-water formation in that region.

While MIS 5e provides insights into North Atlantic-Nordic Seas dynamics during globally warmer-than-present climate conditions, the subsequent glacial inception and transition into the MIS 4 glacial allow the reconstruction of Nordic Seas deep-water dynamics (and its potential role in $CO_{2,atm}$ variations) over both glacial-interglacial and millennial timescales. The MIS 5e/d and MIS 5a/4 transitions are both characterised by a decline in $CO_{2,atm}$ levels of ~35 ppm, i.e., from ~275 to ~240 ppm and from ~240 to ~205 ppm respectively (Bereiter et al., 2015), as well as growing northern-hemisphere ice sheets and a drop in global temperatures (e.g., Grant et al., 2012). MIS 4 was linked with an enhanced chemical separation of intermediate and deep water masses in the Atlantic Ocean, facilitating enhanced carbon sequestration in the Atlantic Ocean interior and a drop in $CO_{2,atm}$ concentrations at that time (e.g., Adkins, 2013; Yu et al., 2016). A decline (rise) in bottom water [CO_3^{2-}] and diminished (enhanced) carbonate preservation in Atlantic sediment cores below (above) 3 km water depth (Broecker and Clark, 2001; Broecker et al., 2015; Yu et al., 2016) indicate a similar water mass stratification during MIS 4 and the LGM (Yu et al., 2008; Ezat et al., 2021). Superimposed on glacial-interglacial climate variability, perturbations in Atlantic overturning and associated northward heat transport were identified during North Atlantic cold phases (i.e., stadials) during the last glacial cycle (e.g., Böhm et al., 2015; Henry et al., 2016). Those stadials associated with iceberg rafting in the North Atlantic, i.e., Heinrich Stadials (HS) (e.g., Hemming, 2004), are associated with a significant decline in planktic foraminiferal stable oxygen isotopes in the Nordic Seas (Rasmussen et al., 1996; Bauch and Weinelt, 1997) and an increase in respired carbon storage in the North Atlantic (Yu et al., 2023). However, the lack of bottom water [CO_3^{2-}] reconstructions in northern high-latitude

regions hampers our understanding of Nordic Seas overturning dynamics and possible impacts on Atlantic overturning and respired carbon accumulation in the past.

Here, we present combined epibenthic foraminiferal (i.e., *Cibicidoides wuellerstorfi*) B/Ca-based bottom water [CO_3^{2-}] reconstructions and stable oxygen and carbon isotopes in marine sediment core PS1243 (6.533°W, 69.367°N, 2711 m water depth) from the Norwegian Sea, to assess changes in deep convection in the Nordic Seas from MIS 5e to MIS 4. A comparison to a compilation of existing bottom water [CO_3^{2-}] records from the Atlantic Ocean covering the last glacial cycle building on earlier efforts (Yu et al., 2008; Yu et al., 2016) and a complementary abundance record of the aragonitic pteropod *Limacina spp.* from PS1243 sediments provides insights into temporal variations in the corrosivity of bottom waters in the Nordic Seas and the vertical position of the aragonite compensation depth that allows possible links to be drawn between shifts in Nordic Seas and Atlantic Ocean overturning and water mass structure.

2. Study area

The hydrography of the Nordic Seas is strongly influenced by the interaction between Atlantic Surface Water (ASW) inflowing from the North Atlantic and Polar Water originating in the Arctic Ocean (Fig. 1). Warm and saline ASW enters the Nordic Seas both east and west of Iceland via the Greenland-Scotland-Ridge (Fig. 1; e.g., Timmermans and Marshall, 2020). The poleward extension of ASW from the North Atlantic Current releases heat to the atmosphere, which leads to surface ocean cooling by up to 7 °C within the Nordic Seas (e.g., Mauritzen et al., 2011; Østerhus et al., 2019). About 70 % (5–6 Sv) of ASW leaves the Nordic Seas after cooling and densification as overflow waters via the Greenland-Scotland-Ridge with Denmark Strait Overflow Water (DSOW) and Iceland-Scotland Overflow Water (ISOW) contributing equally to the combined volume transport of ~13 Sv south of Greenland (Fig. 1; Dickson and Brown, 1994; Østerhus et al., 2019). South of Greenland, Nordic Seas-sourced overflow waters mix with Labrador Sea Water (6–7 Sv) and continue their southward flow as NADW (~20 Sv) (Fig. 1; Dickson and Brown, 1994; Paillet et al., 1998).

Cold and low-salinity Polar Water from the Arctic Ocean enters the Nordic Seas via the western Fram Strait (Fig. 1; e.g., Olafsson et al., 2021). Differences in temperature (T) and salinity (S) between Arctic Ocean- and North Atlantic-sourced waters result in the formation of the Arctic Front (AF, defined by S=35) and the Polar Front (PF, defined by S=34.4) (Fig. 1; Swift and Aagaard, 1981) within the Nordic Seas. The convergence of surface water masses between the PF and AF is intrinsically linked with the formation of cold (T=-1–1 °C) and saline (S=34.4–34.9) deep waters (Fig. 1; Swift and Aagaard, 1981; Schäfer et al., 2001; Zweng et al., 2018). Specifically, deep-water convection is triggered by sea ice formation, surface cooling during winter and dense water supply from the Arctic Ocean resulting from brine rejection on seasonally ice-covered Arctic shelves (Roach et al., 1993; Schott et al., 1993; Marshall and Schott, 1999).

Seawater [CO_3^{2-}] in the central Nordic Seas vary between 120–170 µmol/kg at the surface and 90–100 µmol/kg in bottom waters (Fig. 1b; Lauvset et al., 2022). Deep-water formation in the Nordic Seas results in a weak depth gradient of [CO_3^{2-}] throughout the water column due to the transport of low-CO_2 and high-[CO_3^{2-}] surface waters to depth (Yu et al., 2008; Lauvset

et al., 2022). At present-day, young and high-[CO_3^{2-}] deep-water masses from the Nordic Seas are a major component of NADW, which hence has typical [CO_3^{2-}] of >100 µmol/kg (Fig. 1c; Lauvset et al., 2022). Calcite saturation (Ω_C) levels are above 1 everywhere in the Nordic Seas and in the northern North Atlantic (Fig. 1b, c; Lauvset et al., 2022). In contrast, the transition from aragonite over- to undersaturation (where aragonite saturation (Ω_A) equals 1) occurs at ~2300 m water depth in the North Atlantic and at ~2000 m in the Nordic Seas (Fig. 1b, c; Lauvset et al., 2022).

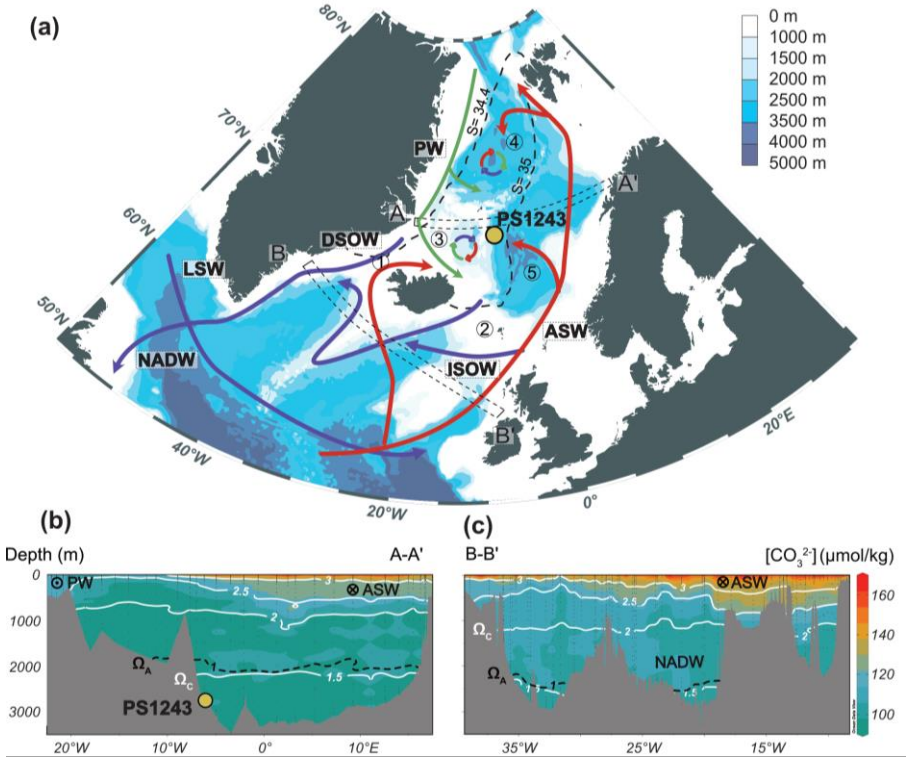

Fig. 1: Oceanographic setting and carbonate system parameters in the Nordic Seas and North Atlantic. (a) Bathymetry with numbers indicating relevant basins and bathymetric features: 1) Denmark Strait, 2) Iceland-Scotland Ridge, 3) Iceland Sea, 4) Greenland Sea and 5) Norwegian Sea. The arrows show warm- (red) and cold (green) surface currents as well as major deep-water circulation pathways (blue). Circles with arrows indicate regions of deep convection. Dashed polygons indicate transects shown in (b) and (c). Dashed lines show isohalines at the surface indicating a salinity (S)=34.4 for the Polar Front and S=35 for the Arctic Front (Zweng et al., 2018). Present-day seawater carbonate ion concentrations ([CO_3^{2-}]) in a west-east transect across b) the Nordic Seas (see A–A' in a) and c) the North Atlantic (see B–B' in a) with contours indicating calcite saturation levels Ω_C (white contours) and the aragonite saturation state of Ω_A=1 (black contour). Seawater [CO_3^{2-}] are uncorrected for any anthropogenic CO_2 uptake. Sections are based on the Global Ocean Data Analysis Project dataset, version 2 (GLODAPv2; Lauvset et al., 2022). Yellow circle shows the location of the study core PS1243.

3. Methods

3.1 Sediment core PS1243

Sediment core PS1243 was retrieved near the foot of Jan Mayen Ridge in the western Norwegian Basin from a water depth of 2711 m (Fig. 1). The site is located close to the modern AF (Fig. 1). The sediment sequence is a stack of gravity core PS1243-1 and the accompanying giant trigger box core PS1243-2. These were combined using the base of the Vedde Ash layer found in both sequences (Bauch et al., 2001). Site PS1243 is currently bathed in Norwegian Sea Deep Water (Swift and Koltermann, 1988) and is ideally suited to monitor variations in the deep convection in the Nordic Seas and Nordic Seas-Atlantic Ocean exchange in combination with other sites from the Atlantic Ocean.

Sediment samples from core PS1243 were taken at 1 cm-slices (25 cm^3), were freeze-dried and washed over a sieve with a mesh size of 63 µm (Bauch et al., 2001). The coarse fraction was subsequently dried at 45–50 °C to be further processed for stable isotope and trace element analyses on foraminifera as well as pteropod abundance estimates.

3.2 Benthic and planktic foraminiferal stable oxygen and carbon isotope analyses

New stable oxygen and carbon isotope measurements were performed on one to five individuals of the epibenthic foraminifer *C. wuellerstorfi* larger than the 125 µm-fraction from 102 samples at the Alfred Wegener Institute, Helmholtz Centre for Polar and Marine Research (AWI) in Bremerhaven (Germany), with a Thermo Finnigan MAT253 isotope ratio mass spectrometer using an automated Kiel carbonate preparation device. Our new data are combined with previously published stable isotope data on *C. wuellerstorfi* performed in core PS1243 (n=127; Bauch et al., 2012). The benthic record is complemented by a continuous isotope record of the planktic foraminifer *Neogloboquadrina pachyderma* (Bauch et al., 2012).

Stable oxygen and carbon isotope analyses are reported in delta-notation ($\delta^{13}C$, $\delta^{18}O$) in ‰ units, referenced against the Vienna Pee Dee Belemnite (VPDB) standard. Long-term reproducibility of new analyses was assessed with an in-house carbonate standard and is <0.04 ‰ for $\delta^{13}C$ and <0.08 ‰ for $\delta^{18}O$. The mean standard deviation of new *C. wuellerstorfi* $\delta^{18}O$ and $\delta^{13}C$ measurements (this study) that replicate published data (Bauch et al., 2012) (n=40) is below 0.06 ‰ VPDB for both $\delta^{13}C$ and $\delta^{18}O$, which is similar to the analytical uncertainties. *C. wuellerstorfi* $\delta^{18}O$ values were corrected by +0.64 ‰ VPDB to account for disequilibrium effects (Shackleton, 1974; Bauch and Erlenkeuser, 2003).

3.3 *C. wuellerstorfi* B/Ca analyses

To measure B/Ca ratios of *C. wuellerstorfi*, 10 to 15 individuals were hand-picked with a dry brush from the sediment fraction larger than 125 µm, resulting in sample weights of 200 to 600 µg $CaCO_3$. In total, 130 samples with sufficient abundance of *C. wuellerstorfi* were analysed. Yet, abundances were insufficient for *C. wuellerstorfi* B/Ca analysis in core sections between 50–103 cm and 114–138 cm (representing parts of MIS 3 and 2). Given low numbers of *C. wuellerstorfi* tests in 6 samples, consecutive samples were combined over a 2 cm-interval.

Foraminiferal tests were treated according to the oxidative cleaning protocol of Barker et al. (2003) in B-free clean laboratory space. Briefly, each *C. wuellerstorfi* specimen was crushed using a scalpel to ensure opening of all chambers without excessive fragmentation. To remove adhering clay, the samples were rinsed several times with ultra-pure water (18.2 MΩ·cm, Milli-Q Q-Pod Element) and methanol. To remove organic matter, samples were oxidatively cleaned using alkali-buffered H_2O_2. Removal of the coarse silicate grains as described in Barker et al. (2003) was not necessary, as microscopically visible silicates were not observed after the oxidative cleaning step. A weak acid leach with 0.001 M ultrapure HNO_3 (prepared from doubly sub-boiled HNO_3) was performed to remove any adsorbed contaminants. The samples were subsequently dissolved in 330 µl 0.1 M HNO_3 to obtain Ca concentrations via inductively coupled plasma-optical emission spectrometry (ICP-OES, ARCOS Spectro) at the Institute of Geosciences, Kiel University (Germany). To reduce the surface adsorption of B and thus minimise the memory effect, the samples were diluted with 0.1 M HF (prepared from ROTIPURAN Ultra 48 %) and 0.3 M HNO_3 to constant 20 µg/g Ca levels (Misra et al., 2014) and then analysed via inductively coupled plasma-mass spectrometry (ICP-MS, Thermo Agilent 7900) at the Institute of Geosciences, Kiel University (Germany). B/Ca ratios were quantified using a set of gravimetrically prepared calibration standards diluted from single element standards (Alfa Aesar and ThermoFisher Scientific). All measurements were normalised using the JCt-1 standard (fossil mid-Holocene giant clam *Tridacna gigas*, B/Ca = 191 µmol/mol; Inoue et al., 2004; Hathorne et al., 2013).

The analytical B/Ca reproducibility determined by repeat measurements of the same sample aliquot (n=11) is σ = 3.3 µmol/mol. The full procedural reproducibility obtained via true replicate samples (n=7) is σ = 4.3 µmol/mol, which is similar to values reported by Yu and Elderfield (2007).

To quantify past bottom water $[CO_3^{2-}]$ at our core site, *C. wuellerstorfi* B/Ca ratios were converted to $[CO_3^{2-}]$ following Eq. (1) after Yu and Elderfield (2007):

$$[CO_3^{2-}]_{down\text{-}core} = [CO_3^{2-}]_{pre\text{-}industrial} + (B/Ca_{down\text{-}core} - B/Ca_{core\text{-}top}) / 1.14, \quad (1)$$

Factor 1.14 is the sensitivity of core-top *C. wuellerstorfi* B/Ca ratio variations (in µmol/mol) per µmol/kg change in bottom water $[CO_3^{2-}]$ (Yu and Elderfield, 2007). Down-core B/Ca values ($B/Ca_{down\text{-}core}$) refer to *C. wuellerstorfi* B/Ca ratios measured in PS1243 downcore. The core-top B/Ca value ($B/Ca_{core\text{-}top}$) represents the average B/Ca ratios of our three uppermost samples (2.5–6.5 cm), representing the late Holocene (mean B/Ca=202±1.2 µmol/mol, 1σ), resulting in $B/Ca_{core\text{-}top}$=202±4.5 µmol/mol taking into account the measurement error of 4.3 µmol/mol. Pre-industrial $[CO_3^{2-}]$ ($[CO_3^{2-}]_{pre\text{-}industrial}$) values at the study site are calculated based on modern bottom water $[CO_3^{2-}]$ ($[CO_3^{2-}]_{modern}$) corrected for seawater $[CO_3^{2-}]$ changes caused by anthropogenic CO_2 emissions to the atmosphere. Because Olsen et al. (2010) and Vázquez-Rodríguez et al. (2009) estimated an anthropogenic dissolved inorganic carbon (DIC) addition of ~8±3 µmol/kg (2σ) and ~12±10 µmol/kg (2σ) for the deep Nordic Seas, respectively, we calculate a mean anthropogenic DIC contribution of 10±6 µmol/mol (2σ) for bottom waters at our study site from both of these estimates. Subtracting this value from modern bottom water DIC levels at the study site (station ID5411 (measured 2009): 2166 µmol/kg; Lauvset et al., 2022) and assuming unchanged bottom water alkalinity (station ID5411 (measured 2009): 2302 µmol/kg; Lauvset et al., 2022), estimated bottom water $[CO_3^{2-}]_{pre\text{-}industrial}$ at the study site is 101±3 µmol/kg (1σ). This implies a $[CO_3^{2-}]$ decrease of ~5±3 µmol/kg (2σ) due to the evasion of anthropogenic CO_2

into the deep Norwegian Sea. The total uncertainty of 9.3 µmol/kg (1σ) for our B/Ca derived $[CO_3^{2-}]_{down\text{-}core}$ values results from 1σ-uncertainties for $[CO_3^{2-}]_{pre\text{-}industrial}$=5.6 µmol/kg, $B/Ca_{down\text{-}core}$=4.3 µmol/mol, $B/Ca_{core\text{-}top}$=4.5 µmol/mol as well as the calibration error of 5 µmol/kg (1σ; Yu and Elderfield, 2007; Yu et al., 2008). For $[CO_3^{2-}]$ calculations, we used the CO_2Sys software package (version 2.1) of Pierrot et al. (2011) with solubility constants K_1 and K_2 for carbonic acid by Mehrbach et al. (1973), refitted by Dickson and Millero (1987). The dissociation constant for sulfate (K_{SO4}) was used according to Dickson (1990) and the total boron concentration in seawater was calculated after Uppström (1974). In order to assess linkages between deep-water formation and overturning dynamics in the Nordic Seas and the Atlantic Ocean, we compare our new bottom water $[CO_3^{2-}]_{down\text{-}core}$ record from the deep Norwegian Sea with similar records from the Atlantic Ocean (Table 1).

Table 1: Compilation of benthic foraminiferal B/Ca-based bottom water $[CO_3^{2-}]$ records from the Atlantic Ocean obtained via laser ablation (LA)- or solution-based inductively coupled plasma mass spectrometry (ICP-MS) analysis. *Core VM28-122 and ODP Site 999 record intermediate water dynamics of the Atlantic Ocean due to the shallow sill depth at ~1.8 km water depth of the Caribbean Sea despite their retrieval from a water depth of 3623 m and 2839 m, respectively. Core numbers refers to core labels in Figs. 6 and 9.

Core number	Core	Latitude	Longitude	Water depth (m)	Analytical approach	Benthic foraminiferal species	Reference(s)	Age range of B/Ca analyses (ka BP)
1	PS1243	69.37°N	6.55°W	2711	ICP-MS	*C. wuellerstorfi*	This study	1–130
2	NEAP8K	59.79°N	23.90°E	2360	ICP-MS	*C. wuellerstorfi*	Yu et al., 2008	0–40
3	BOFS17K	58.00°N	16.50°E	1150	ICP-MS	*C. mundulus*	Yu et al., 2008	0–34
4	ODP Site 980	55.49°N	14.70°W	2184	ICP-MS	*C. wuellerstorfi*	Chalk et al., 2019; Crocker et al., 2016	4–145 0–40
5	BOFS11K	55.19°N	20.34°E	2004	ICP-MS	*C. wuellerstorfi*	Yu et al., 2008	0–36
6	BOFS10K	54.67°N	20.65°E	2761	ICP-MS	*C. wuellerstorfi*	Yu et al., 2008	0–20
7	BOFS8K	52.50°N	22.06°E	4045	ICP-MS	*C. wuellerstorfi*	Yu et al., 2008, 2010b	7–37
8	BOFS5K	50.69°N	21.86°E	3547	ICP-MS	*C. wuellerstorfi*	Yu et al., 2008	1–32
9	U1308	49.88°N	24.24°W	3871	ICP-MS	*C. wuellerstorfi*	Chalk et al., 2019	0–130
10	U1313	41.00°N	32.96°W	3426	ICP-MS	*C. wuellerstorfi*	Chalk et al., 2019	5–137
11	MD95-2039	40.58°N	10.35°W	3381	ICP-MS	*C. wuellerstorfi*	Yu et al., 2023	0–150
12	MD01-2446	39.38°N	16.01°W	3576	ICP-MS	*C. wuellerstorfi*	Yu et al., 2016	51–87
13	ODP Site 999*	12.74°N	78.74°W	2839*	ICP-MS	*C. wuellerstorfi*	Chalk et al., 2019	4–130

14	VM28-122*	11.93°N	78.68°W	3623*	ICP-MS	*C. wuellerstorfi*	Yu et al., 2010a,b	3–160
15	KNR197-3-46CDH	7.45°N	53.67°W	950	ICP-MS	*C. pachyderma*	Oppo et al., 2023	5–23
16	EW9209-2JPC	5.60°N	44.40°W	3528	ICP-MS	*C. wuellerstorfi*	Yu et al., 2016	50–92
17	RC16-59	4.00°N	43.00°N	3520	ICP-MS	*C. wuellerstorfi*	Broecker et al., 2015	0–158
18	GeoB1115-3	3.56°S	12.56°W	2945	LA-ICP-MS	*C. wuellerstorfi*	Raitzsch et al., 2011	8–135
19	GeoB1118-3	3.56°S	16.42°W	4671	LA-ICP-MS	*C. wuellerstorfi*	Raitzsch et al., 2011	10–135
20	GeoB1117-2	3.81°S	14.89°W	3984	LA-ICP-MS	*C. wuellerstorfi*	Raitzsch et al., 2011	8–135
21	RC13-228	22.33°S	11.20°E	3204	ICP-MS	*C. wuellerstorfi*	Yu et al., 2016	47–88
22	RC13-229	25.49°S	11.31°E	4191	ICP-MS	*C. wuellerstorfi*	Yu et al., 2016	47–101
23	KNR159-5-90GGC	27.35°S	46.64°W	1105	ICP-MS	*C. pachyderma*	Lacerra et al., 2019	8–22
24	KNR159-5-78GGC	27.48°S	46.33°W	1820	ICP-MS	*C. wuellerstorfi*	Lacerra et al., 2017	4–25
25	KNR159-5-33GGC	27.57°S	46.18°W	2082	ICP-MS	*C. wuellerstorfi*	Lacerra et al., 2017	1–20
26	ODP Site 1267	28.10°S	1.71°E	4350	ICP-MS	*C. wuellerstorfi*	Kirby et al., 2020	0–40
27	TN057-21	41.13°S	8.80°E	4981	ICP-MS	*C. wuellerstorfi*	Yu et al., 2014; Yu et al., 2016	4–28 52–90
28	MD07-3076	44.15°S	14.23°E	3770	ICP-MS	*C. kullenbergi*	Gottschalk et al., 2015	0–66

3.4. Determination of pteropod abundances

We assessed aragonitic shell abundance changes (i.e., weight percentages) of the dominant pelagic pteropod *Limacina spp.* occurring in PS1243 sediments using the 150–500 µm size fraction. Because of the delicacy of pteropod shells, fragments comprise the main portion and were found continuously in every sample between 86 and 189 cm (i.e., from ~31–98 ka). Where available, more complete shells show a clear predominance of the polar cold-water species *Limacina helicina*, along with occasional abundances of the warmer boreal-subarctic species *Limacina retroversa*. Both species are a common part of the polar pelagic fauna today (Bauerfeind et al., 2014). Sediment samples were weighed and split on a glass plate using a razor blade. Shells and fragments were separated from the sample aliquot and weighed with a Sartorius AC121S analytical balance with an accuracy of 0.1 mg in order to calculate the total weight percentage of *Limacina spp.* fragments in the 150–500 µm fraction.

3.5. Age model

The age model for the continuously sampled core PS1243 is primarily based on planktic foraminiferal $\delta^{18}O$ compared to the benthic $\delta^{18}O$ stack record (LS16; Lisiecki and Stern, 2016). The stratigraphic alignment was established using a 5 cm-running average of the *N. pachyderma* $\delta^{18}O$ record (Fig. 2a, b). We consider ad-hoc uncertainties for the five resulting age markers of 2.5 ka (Table 2) considering uncertainties in the alignment itself (~1.5 kyr) and the possibility of regional phase lags in foraminiferal $\delta^{18}O$ (~2 kyr; Lisiecki and Stern, 2016). Millennial-scale (i.e., short-term) variability in the *N. pachyderma* $\delta^{18}O$ record likely results from the influence of low-$\delta^{18}O$ meltwater events during HSs, as commonly assumed for the Nordic Seas (e.g., Rasmussen et al., 1996; Bauch and Weinelt, 1997; Thornalley et al., 2015). To obtain additional age constraints, we calculated a residual *N. pachyderma* $\delta^{18}O$ record (i.e., subtracted the long-term glacial-interglacial $\delta^{18}O$ variability based on the 5 cm-running average). Using the age model constraints based on our stratigraphic alignment to Lisiecki and Stern (2016), we identified residual $\delta^{18}O$ minima that broadly coincide with HS recorded in the NGRIP $\delta^{18}O$ record (NGRIP member, 2004; Capron et al., 2021) and with peaks in ice rafted detritus (IRD) supply to PS1243 (Bauch et al., 2012). We then aligned these with mid-points of low-$\delta^{18}O$ phases in the NGRIP $\delta^{18}O$ record representing HSs on the AICC2012 ice age scale (Fig. 2; Veres et al., 2013). This premise is consistent with the age model for core PS1243 developed for the last 30 ka of Thornalley et al. (2015). To aid identification of HSs recorded via *N. pachyderma* $\delta^{18}O$ minima for this age model fine-tuning, we use those *N. pachyderma* $\delta^{18}O$ minima that exceed 1σ of the residual record and approach or cross 2σ level (i.e., those with excursions larger than 0.15 ‰ VPDB; Fig. 2). One exception is HS7a that is close to the MIS 5a/4-tie point based on the $\delta^{18}O$ alignment to Lisiecki and Stern (2016) that, if included, might cause large and unrealistic shifts in sedimentation rates (Fig. 2). We consider uncertainties in selecting HS mid-points in the residual *N. pachyderma* $\delta^{18}O$ and their equivalents in the NGRIP $\delta^{18}O$ record to be half the duration of the respective HS in the NGRIP $\delta^{18}O$ record each (Capron et al., 2021), which then propagate to the full age marker uncertainties given in Table 2. We adopt the HS numbering from Yu et al. (2023), noting that it may differ from the naming conventions applied in other studies, particularly for HS older than HS6. Our age model concurs with two northern hemisphere volcanic event marker layers identified in PS1243: the Vedde ash at 44.5 cm (12.1 ka BP; Mortensen et al., 2005; Rasmussen et al., 2006; Fig. 2) and an ash layer considered to reflect the North Atlantic Z2 ash at 133 cm (56.1 ka BP; Groen and Storey, 2022; Fig. 2). Core PS1243 was shown to resolve millennial-scale variations in surface ocean hydrography in the Norwegian Sea despite low sedimentation rates between 1–4 cm/ka, which likely results from high foraminiferal abundances, excellent carbonate preservation and/or low bioturbation depths (Fig. 2c–f; e.g., Bauch et al., 2012; Thornalley et al., 2015).

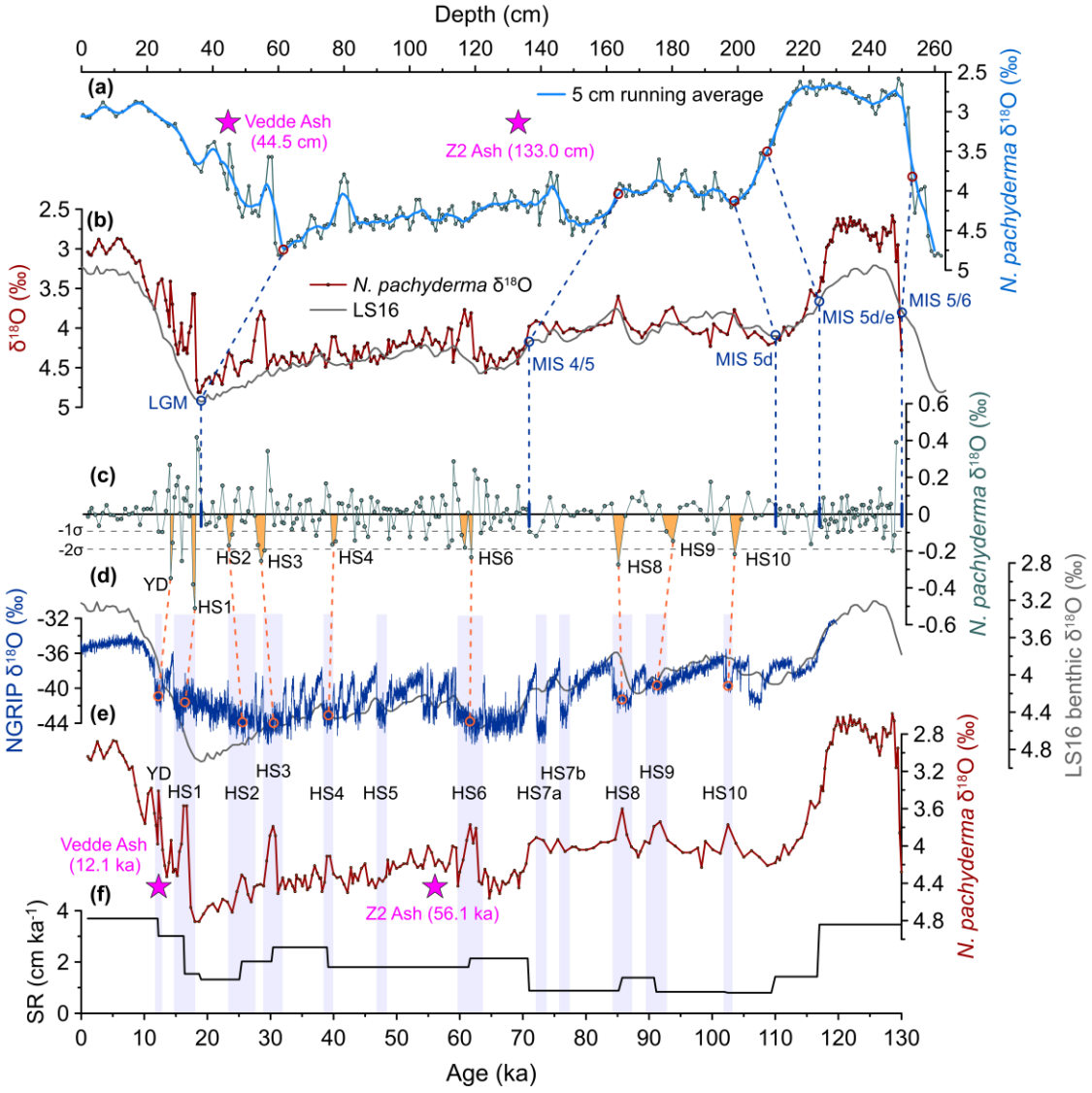

Fig. 2: Age model for sediment core PS1243 based on a stratigraphic alignment of *N. pachyderma* $\delta^{18}O$ changes to the benthic $\delta^{18}O$ stack (LS16) of Lisiecki and Stern (2016) and water isotope variations ($\delta^{18}O$) of the Greenland NGRIP ice core (NGRIP Members, 2004) on the AICC2012 ice age scale (Veres et al., 2013). (a) *N. pachyderma* $\delta^{18}O$ record of PS1243 (grey) and its 5 cm-running average (blue) plotted against depth (top axis; in ‰ versus the Vienna Peedee Belemnite (VPDB) standard). (b) LS16 (grey) and stratigraphically aligned *N. pachyderma* $\delta^{18}O$ in PS1243 (red), based on tie points between the two (open circles and dashed lines, Table 2). (c) Residual *N. pachyderma* $\delta^{18}O$ record of PS1243 (5 cm-running average subtracted). The horizontal dashed lines indicate the 1σ-and 2σ–standard deviation of the residual record of 1σ=0.097 ‰ and 2σ=0.194 ‰, respectively. Blue lines show established tie points based on LS16 (a, b). Orange areas display short *N. pachyderma* $\delta^{18}O$ minima that are interpreted to represent Heinrich stadials (HS1–4, 6, 8–10) and the Younger Dryas (YD), following the rationale of Thornalley et al. (2015); this forms the basis for an additional chronostratigraphic fine-tuning through a stratigraphic alignment of residual *N. pachyderma* $\delta^{18}O$ minima to HSs identified in the NGRIP $\delta^{18}O$ record (Guillevic et al., 2014; Capron et al., 2021) (orange open circles and dashed lines in d, Table 2; see uncertainty assessment in section 3.5). (d) NGRIP $\delta^{18}O$ variations (NGRIP Members, 2004; blue) on the AICC2012 ice age scale (Veres et al., 2013) and the benthic foraminiferal $\delta^{18}O$ stack of LS16 (Lisiecki and Stern, 2016; grey). Stars show the occurrence of the Vedde ash in PS1243 at 44.5 cm and an ash layer considered to reflect the North Atlantic Z2 ash at 133 cm – both independently

dated to 12.1 ka BP (Mortensen et al., 2005; Rasmussen et al., 2006) and 56.1 ka BP (Groen and Storey, 2022), respectively. Light blue bars indicate HSs following the timing given in Capron et al. (2021). HS numbering follows Yu et al. (2023), which may differ from the naming convention in other studies, especially for HS older than HS6. e) *N. pachyderma* $\delta^{18}O$ in study core PS1243 on the final age model (combining the stratigraphic alignments in (a)–(d)), and (f) resulting sedimentation rate (SR) changes. (b)–(f) are shown against age (bottom axis). MIS–Marine Isotope Stage.

Table 2: Tie points of the established age model for sediment core PS1243. The calibrated core-top radiocarbon age is reported in Bauch and Weinelt (1997). Tuning targets of *N. pachyderma* $\delta^{18}O$ variations in core PS1243 encompass the LS16 benthic foraminiferal $\delta^{18}O$ stack from Lisiecki and Stern (2016) and NGRIP $\delta^{18}O$ variations (NGRIP Members, 2004 on the AICC2012 ice age scale, Veres et al., 2013). The onset of MIS 5e (*sensu stricto*) was defined in the study core after Bauch et al. (2012) as the end of ice-rafted detritus input following MIS 6. YD – Younger Dryas, HS – Heinrich Stadial, MIS – Marine Isotope Stage

Event	Depth (cm)	Age (ka BP)	Error (±ka)	Tuning target
Core-top	1.5	1.3	0.1	^{14}C dated
YD	45.0	12.3	0.7	NGRIP $\delta^{18}O$
HS1	57.5	16.4	2.4	NGRIP $\delta^{18}O$
LGM	61.5	19.0	2.5	LS16
HS2	70.0	25.5	3.1	NGRIP $\delta^{18}O$
HS3	80.0	30.4	2.1	NGRIP $\delta^{18}O$
HS4	102.5	39.2	1.1	NGRIP $\delta^{18}O$
HS6	143.0	61.7	2.8	NGRIP $\delta^{18}O$
MIS 4/5	163.0	71.0	2.5	LS16
HS8	176.0	85.8	2.3	NGRIP $\delta^{18}O$
HS9	183.5	91.2	2.4	NGRIP $\delta^{18}O$
HS10	193.0	102.5	1.0	NGRIP $\delta^{18}O$
MIS 5d	199.0	110.0	2.5	LS16
MIS 5d/e	209.0	117.0	2.5	LS16
Onset MIS 5e (*sensu stricto*)	240.0	126.0	2.5	interpolated
MIS 5/6	254.0	130.0	2.5	LS16

4. Results

4.1 Efficiency of benthic foraminiferal cleaning for B/Ca analysis

The reconstruction of bottom water conditions based on element/Ca ratios in benthic foraminiferal calcite can be affected by post-depositional contamination and the presence of Mn-carbonate or Mn-Fe oxyhydroxide overgrowths or non-removed clay detritus on or inside foraminiferal tests (e.g., Boyle, 1983; Barker et al., 2003; Misra et al., 2014). To evaluate the efficiency of the applied cleaning for our *C. wuellerstorfi* B/Ca analysis, we assess *C. wuellerstorfi* Al/Ca and Mn/Ca levels and their co-variation with *C. wuellerstorfi* B/Ca ratios in our samples (Fig. 3). *C. wuellerstorfi* Mn/Ca are mostly below 100 µmol/mol

(Fig. 3a), which is considered a benchmark for samples unbiased by contamination (Boyle, 1983). In addition, we do not observe a statistically significant correlation between *C. wuellerstorfi* Mn/Ca and B/Ca values (R=0.01, *p*=0.9; Fig. 3b) and *C. wuellerstorfi* Al/Ca and B/Ca ratios within 95%-confidence levels (R=0.1, *p*=0.2; Fig. 3d). Along with the fact that our *C. wuellerstorfi* Al/Ca are consistently low (Fig. 3c) and frequently below the limit of detection (i.e., Al/Ca<11 µmol/mol; n=38), we consider contamination of our B/Ca data to be negligible.

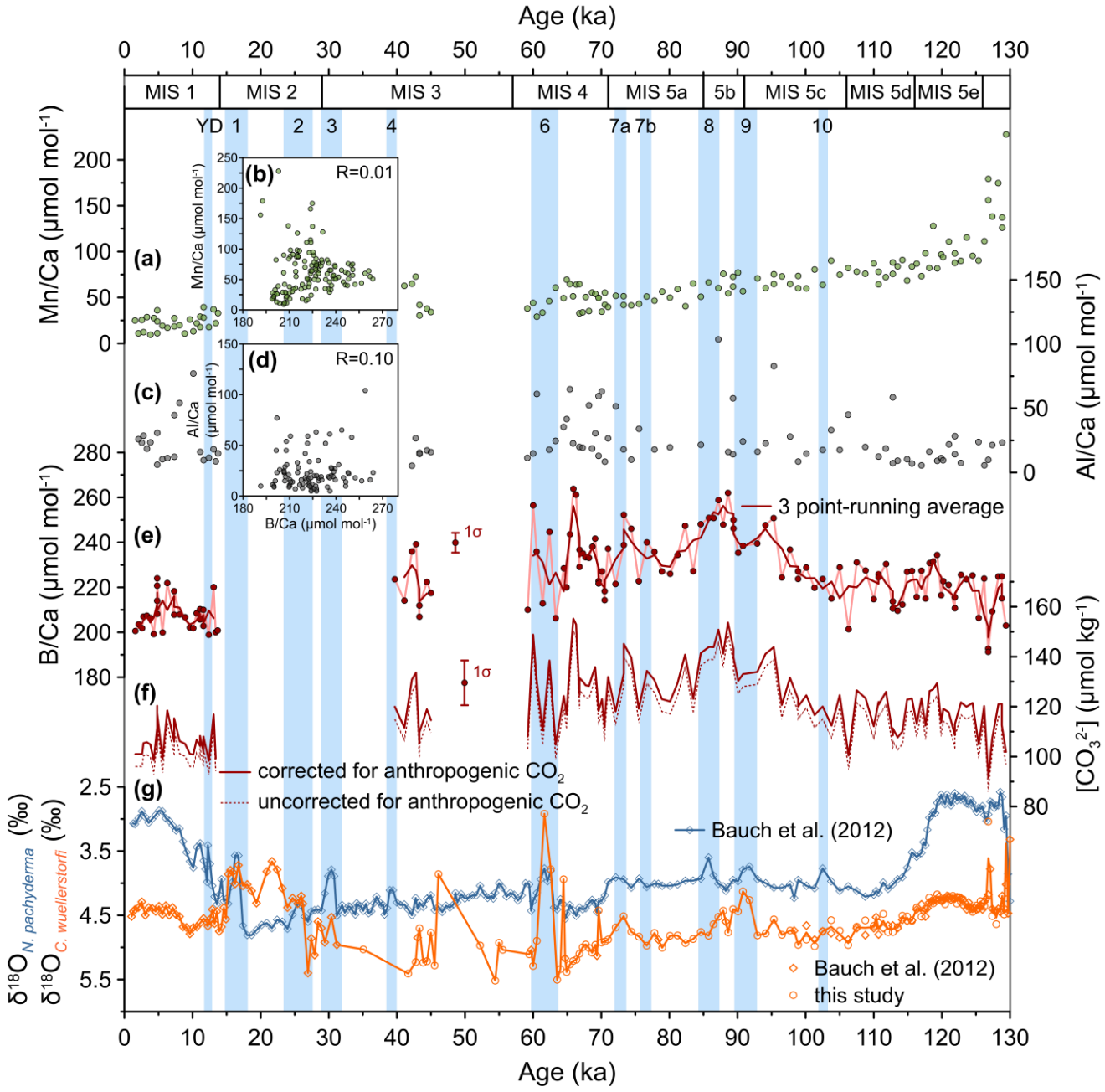

Fig. 3: Foraminiferal trace element and stable oxygen isotope variations during the last glacial cycle in core PS1243. (a) *C. wuellerstorfi* Mn/Ca and (b) cross-plotted against *C. wuellerstorfi* B/Ca ratios, (c) *C. wuellerstorfi* Al/Ca and (d) cross-plotted against *C. wuellerstorfi* B/Ca ratios. (e) *C. wuellerstorfi* B/Ca ratios (error bar indicates the mean 1σ-uncertainty of $B/Ca_{down\text{-}core}$=4.3 µmol/mol), (f) *C. wuellerstorfi* B/Ca-based $[CO_3^{2-}]$ reconstructions down-core based on modern and pre-industrial bottom water $[CO_3^{2-}]$ values represented by our three core-top values (2.5–6.5 cm; error bar indicates the mean 1σ-uncertainty of $[CO_3^{2-}]_{down\text{-}core}$=9.3 µmol/kg). (g) *C. wuellerstorfi* $\delta^{18}O$ and *N. pachyderma* $\delta^{18}O$ from Bauch et al. (2012) and this study. Boxes at the top indicate marine isotope stages (MIS) according to Lisiecki and Raymo (2005) and marine isotope substages (MIS 5e–5a) after Railsback et al. (2015). Blue bars and numbers indicate Heinrich stadials (HS) and the Younger Dryas (YD) following Capron et al. (2021). The

onset of MIS 5e (*sensu stricto*) was defined in the study core after Bauch et al. (2012) as the end of ice-rafted detritus input following MIS 6.

4.2. *C. wuellerstorfi* $\delta^{13}C$ and $[CO_3^{2-}]$ variability during MIS 5 and 4

During late MIS 5 and MIS 4, *C. wuellerstorfi* B/Ca-derived $[CO_3^{2-}]$ at site PS1243 are generally higher than during the Holocene (mean $[CO_3^{2-}]$=107±7 µmol/kg (1σ), n=19) and $[CO_3^{2-}]_{pre\text{-}industrial}$ at the core site (101±3 µmol/kg (1σ); Fig. 4). During MIS 5e (119±7 µmol/kg (1σ); n=16) and 5d (117±8 µmol/kg (1σ); n=13), reconstructed bottom water $[CO_3^{2-}]$ estimates in the deep Norwegian Sea are only slightly higher than the Holocene mean, yet these differences are statistically significant within 95% confidence level based on a two-sided student *t*-test (p<0.01; Fig. 4). In addition, we find a statistically significant correlation between *C. wuellerstorfi* $\delta^{13}C$ and bottom water $[CO_3^{2-}]$ (R^2=0.58, p<0.01) over the last glacial cycle in the interval covered by our analyses (Fig. 5). High bottom water $[CO_3^{2-}]$ characterise MIS 4 (127 ±13 µmol/kg (1σ), n=23) and MIS 5b (142 ±7 µmol/kg (1σ), n=9), which coincides with high *C. wuellerstorfi* $\delta^{13}C$ values during these times (Figs. 4, 5). In other words, both *C. wuellerstorfi* $\delta^{13}C$ and bottom water $[CO_3^{2-}]$ show elevated values despite a lowering of $CO_{2,atm}$ (Figs. 4, 5).

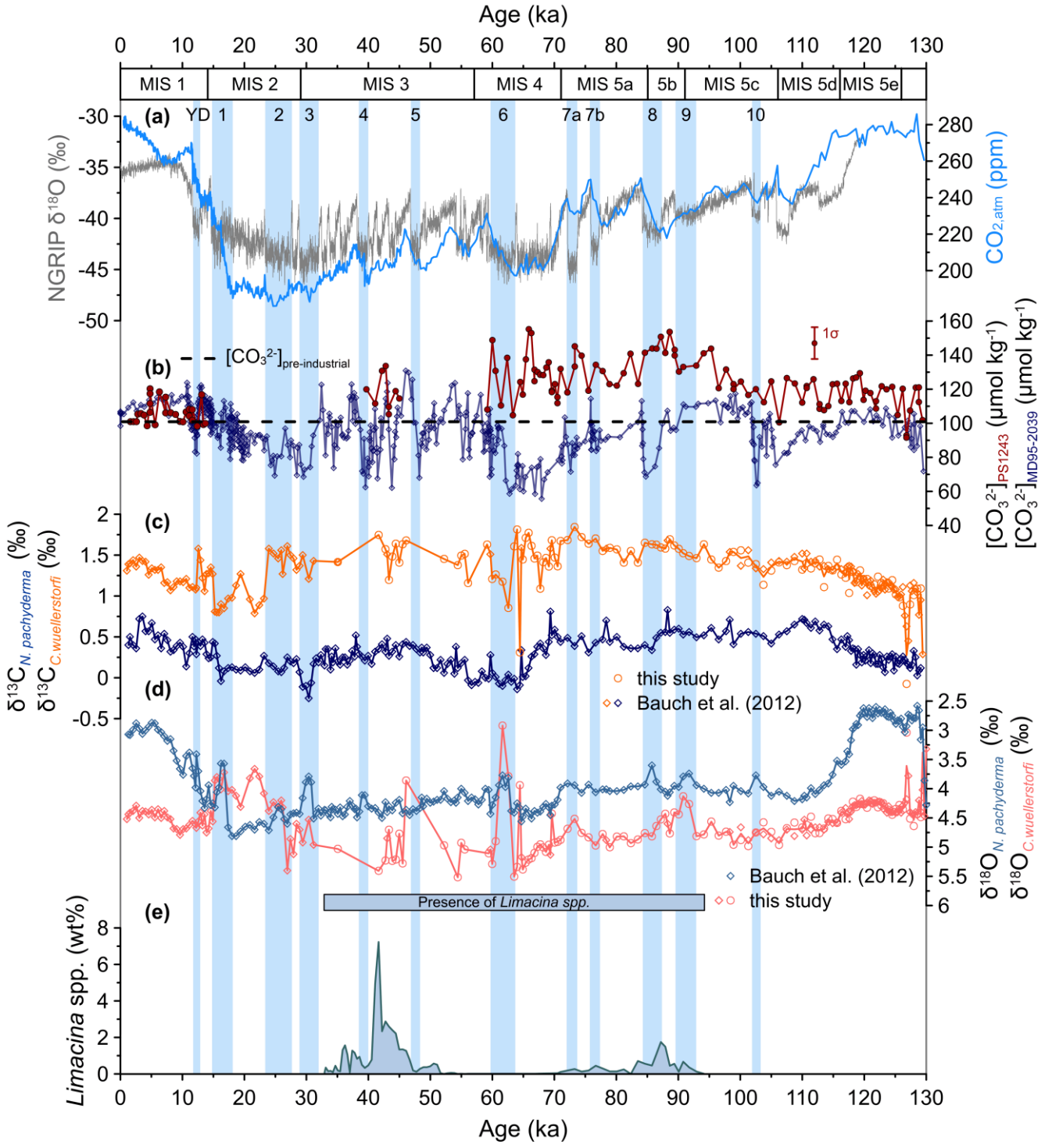

Fig. 4: Multi-proxy bottom water reconstructions in sediment core PS1243 during the last glacial cycle compared to other proxy records. (a) Water isotope variations ($\delta^{18}O$) in the Greenland NGRIP ice core (NGRIP Members, 2004) on the AICC2012 ice age

scale (Veres et al., 2013) and atmospheric CO_2 concentrations (Bereiter et al., 2015). (b) Bottom water [CO_3^{2-}] records of cores PS1243 (this study; red) and MD95-2039 from the Iberian margin (Yu et al., 2023; blue). Error bar indicates the mean 1σ-uncertainty of [CO_3^{2-}]$_{down\text{-}core}$=9.3 µmol/kg in PS1243. (c) $\delta^{13}C$ and (d) $\delta^{18}O$ of *C. wuellerstorfi* (orange) and *N. pachyderma* (blue) in core PS1243. (e) *Limacina spp.* weight percentages in PS1243. Boxes at the top indicate marine isotope stages (MIS) according to Lisiecki and Raymo (2005) and marine isotope substages (MIS 5e–5a) following Railsback et al. (2015). Blue bars and numbers indicate the Younger Dryas (YD) and Heinrich stadials (HS) following Capron et al. (2021). The onset of MIS 5e (*sensu stricto*) was defined in the study core after Bauch et al. (2012) as the end of ice-rafted detritus input following MIS 6.

Reconstructed bottom water [CO_3^{2-}] at site PS1243 increase slightly from MIS 5d to MIS 5c/b, which is paralleled by a similar yet more steady rise in *C. wuellerstorfi* $\delta^{13}C$ (Fig. 4). This bottom water [CO_3^{2-}] increase also coincides with increased weight percentages of *Limacina* spp., both reaching a peak in MIS 5b (Fig. 4). However, a rise in *N. pachyderma* $\delta^{13}C$ values during MIS 5d precedes the rise in bottom water [CO_3^{2-}] during MIS 5c (Fig. 4). On average, bottom water [CO_3^{2-}] variations obtained from core PS1243 are offset by 22±9 µmol/kg from bottom water [CO_3^{2-}] reconstructed in Iberian margin core MD95-2039 during MIS 5e and 5d (Fig. 4; Yu et al., 2023). During MIS 5c, coinciding with HS 10, reconstructed bottom water [CO_3^{2-}] variability at both sites shows a divergence towards higher (lower) bottom water [CO_3^{2-}] values in core PS1243 (MD95-2039) (Fig. 4). At that time, both records tend to anti-correlate on millennial timescales, although the temporal resolution is lower in core PS1243 (Fig. 4). Nonetheless, HS8, 7b and 7a are characterised by high-[CO_3^{2-}] bottom waters in Norwegian Sea core PS1243 (this study) and by low-[CO_3^{2-}] bottom waters in core MD95-2039 (Fig 4; Yu et al., 2023). From MIS 5b to 5a, bottom water [CO_3^{2-}] in the deep Norwegian Sea slightly decline and increase by ~25 µmol/kg up to 155 µmol/kg during MIS 4, when core MD95-2039 indicates a bottom water [CO_3^{2-}] minimum of ~60 µmol/kg (Fig. 4; Yu et al., 2023). While during MIS 4 *N. pachyderma* $\delta^{13}C$ values decline and *Limacina* spp. weight percentages decrease to near zero (albeit fragments are still present), *C. wuellerstorfi* $\delta^{13}C$ values remain high with short-term minima only (Fig. 4).

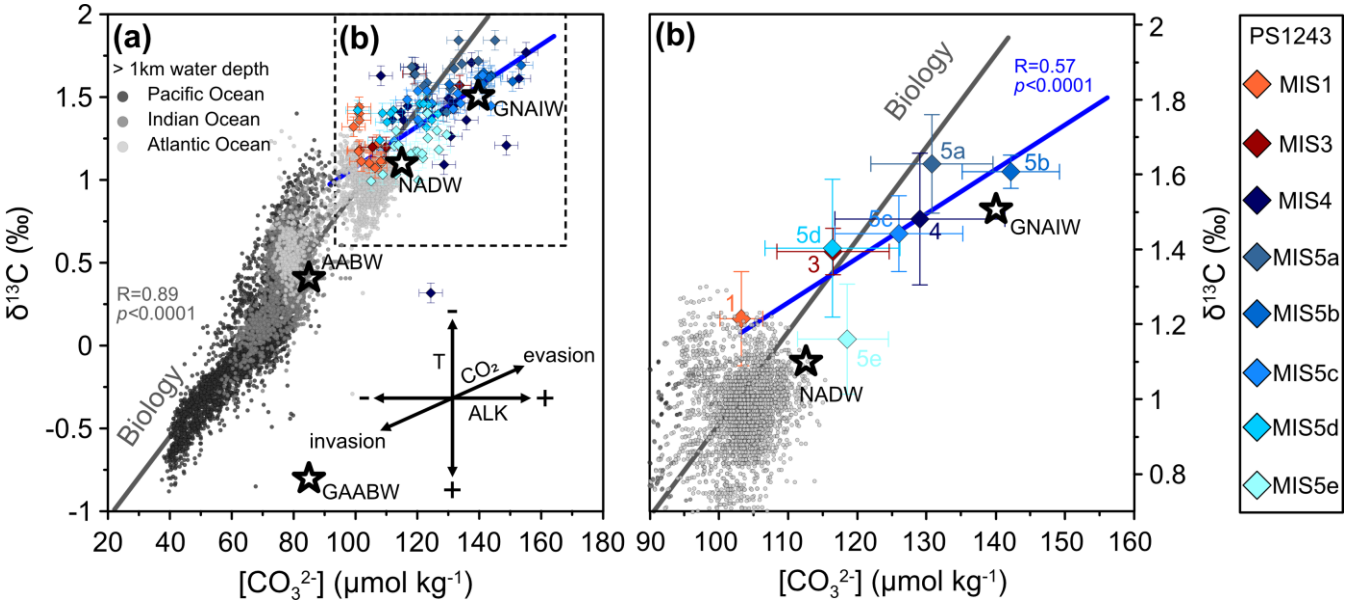

Fig. 5: Correlation of *C. wuellerstorfi* $\delta^{13}C$ and B/Ca-based $[CO_3^{2-}]$ estimates in sediment core PS1243. (a) Modern seawater $\delta^{13}C$ and $[CO_3^{2-}]$ (Lauvset et al., 2022). Black stars indicate endmember values of North Atlantic Deep Water (NADW), Antarctic Bottom Water (AABW), Glacial North Atlantic Intermediate Water (GNAIW) and Glacial Antarctic Bottom Water (GAABW) after Yu et al. (2008; 2020). Diamonds indicate paired *C. wuellerstorfi* $\delta^{13}C$ and B/Ca-based $[CO_3^{2-}]$ estimates in core PS1243 (color-coded according to time interval) with blue line showing a linear regression of the downcore data. (b) Averaged *C. wuellerstorfi* $\delta^{13}C$ and B/Ca-based $[CO_3^{2-}]$ estimates (stippled box in a) for marine isotope stages (MIS) and substages following Lisiecki and Raymo (2005) and Railsback et al. (2015), respectively (color-coded according to the time interval), with blue line indicating the linear regression. Grey lines in a) and b) show the Redfield slope, while vectors in the right-bottom corner of panel (a) indicate an increase in seawater $\delta^{13}C$ with decreasing temperature (T), an increase in $[CO_3^{2-}]$ with rising alkalinity (ALK) and increases in both $[CO_3^{2-}]$ and seawater $\delta^{13}C$ with CO_2 evasion/invasion to/from the atmosphere (Yu et al. 2008).

4.3. Comparison of bottom water $[CO_3^{2-}]$ records from the Atlantic Ocean and the Norwegian Sea

During MIS 5b, 5a and 4, bottom water $[CO_3^{2-}]$ in core PS1243 are generally higher (often by more than ~20 µmol/kg) than reconstructed bottom water $[CO_3^{2-}]$ in the Atlantic Ocean deeper than 3 km water depth (Table 1), except for Site U1313 (~3.4 water depth) whose $[CO_3^{2-}]$ record partly matches that of PS1243 during those times (Fig. 6; Chalk et al., 2019). Above 3 km water depth in the Atlantic Ocean, high bottom water $[CO_3^{2-}]$ similar to those recorded in core PS1243 are only observed in sediment cores VM28-122 (~1.8 km water depth; Yu et al., 2010) and at ODP Site 999 in the Caribbean Sea (~1.8 km; Chalk et al., 2019) as well as at ODP Site 980 in the Northeast Atlantic (~2.2 km; Fig. 6c; Crocker et al., 2016; Chalk et al., 2019). Considering uncertainties of ~10 µmol/kg (1σ) of bottom water $[CO_3^{2-}]$ reconstructions, most North Atlantic records including PS1243 seem to broadly converge during MIS 5e independent from the water depth of the core site, although slight offsets between individual records may occur (Fig. 6).

Reconstructed bottom water $[CO_3^{2-}]$ in core PS1243 are statistically indistinguishable (p=0.44) during MIS 5a and MIS 4 (Fig. 6). In contrast, most Atlantic sediment cores with $[CO_3^{2-}]$ estimates for the water column below 3 km water depth (Table 1) record a decrease in bottom water $[CO_3^{2-}]$ from MIS 5a to MIS 4 (Fig. 6), which is consistent with Yu et al. (2016). This includes sediment cores from the eastern (MD95-2039, MD01-2446) and central North Atlantic (U1308 and U1313), the equatorial Atlantic (RC16-95 and EW9209-2JPC) and the South Atlantic (RC13-229, RC13-228, MD07-3076 and TN057-21) (Fig. 6, Table 1). The deep Atlantic sediment cores MD95-2039 (~3.4 km, Yu et al., 2023) and TN057-21 (~5 km, Yu et al., 2016) with sufficient millennial-scale resolution indicate low bottom water $[CO_3^{2-}]$ during most stadial conditions of MIS 5 (Fig. 6). This is consistent with persistently low stadial $[CO_3^{2-}]$ in the deep South Atlantic during MIS 3 observed in core MD07-3076 (Gottschalk et al., 2015). In contrast, bottom water $[CO_3^{2-}]$ estimates in PS1243 from the deep Norwegian Sea do not show a marked $[CO_3^{2-}]$ decline during stadial periods but rather a slight increase before or during HS periods in MIS 5 (Fig. 4, 6). Given the low sedimentation rate of our study core, the uncertainties of our bottom water $[CO_3^{2-}]$ estimates and the smoothing effect of bioturbational overprints, we consider this to point at either an attenuated positive HS $[CO_3^{2-}]$ anomaly, the lack of an HS $[CO_3^{2-}]$ anomaly or the complete removal of a negative HS $[CO_3^{2-}]$ anomaly via strong smoothing.

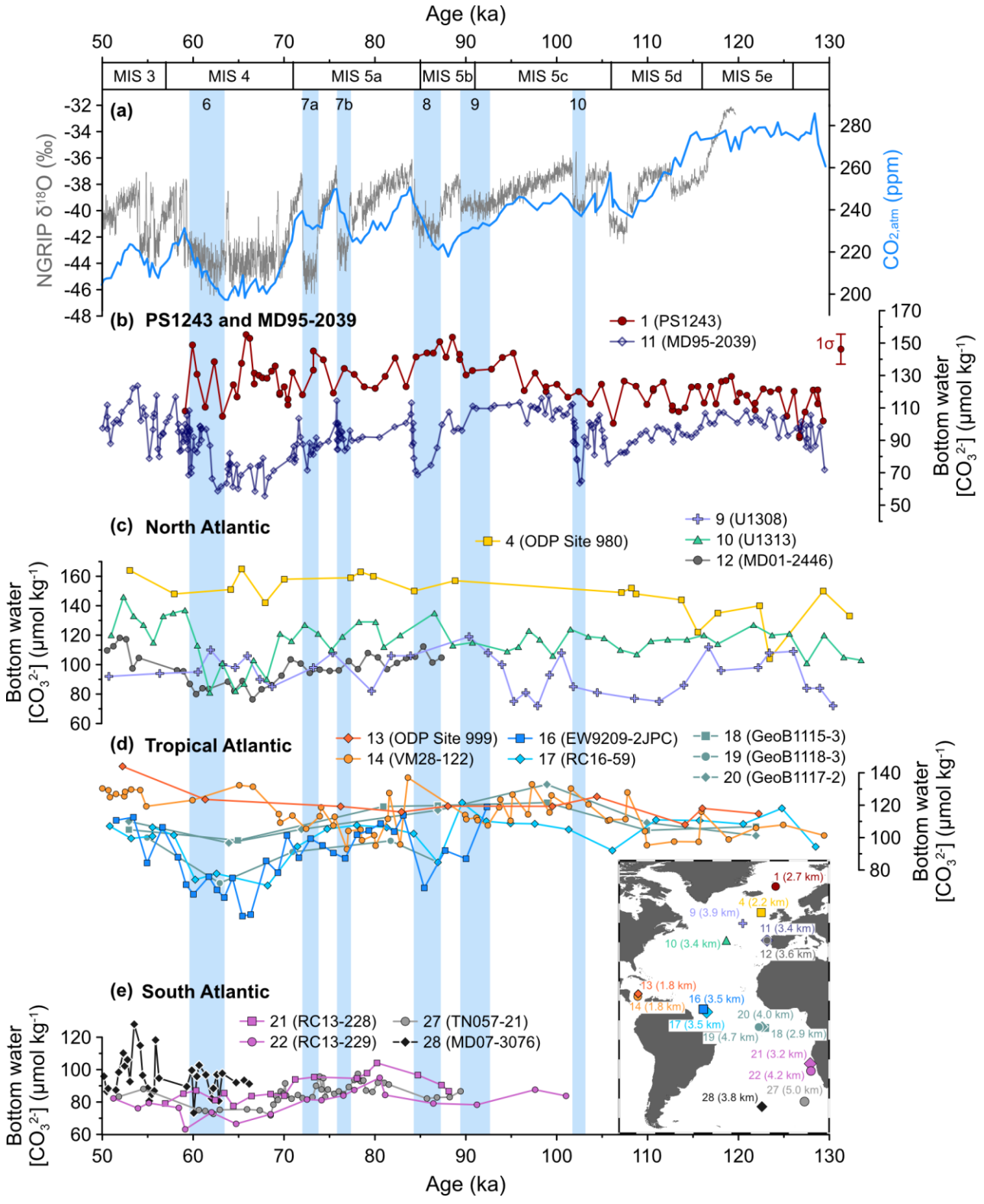
Age (ka)
MIS 3
MIS 4
MIS 5a
MIS 5b
MIS 5c
MIS 5d
MIS 5e
6
7a
7b
8
9
10
(a)
NGRIP δ18O (‰)
CO2,atm (ppm)
(b) PS1243 and MD95-2039
1 (PS1243)
11 (MD95-2039)
1σ
Bottom water [CO3 2-] (µmol kg-1)
(c) North Atlantic
4 (ODP Site 980)
9 (U1308)
10 (U1313)
12 (MD01-2446)
(d) Tropical Atlantic
13 (ODP Site 999)
14 (VM28-122)
16 (EW9209-2JPC)
17 (RC16-59)
18 (GeoB1115-3)
19 (GeoB1118-3)
20 (GeoB1117-2)
1 (2.7 km)
4 (2.2 km)
9 (3.9 km)
11 (3.4 km)
10 (3.4 km)
12 (3.6 km)
13 (1.8 km)
14 (1.8 km)
16 (3.5 km)
20 (4.0 km)
17 (3.5 km)
19 (4.7 km)
18 (2.9 km)
21 (3.2 km)
22 (4.2 km)
27 (5.0 km)
28 (3.8 km)
(e) South Atlantic
21 (RC13-228)
22 (RC13-229)
27 (TN057-21)
28 (MD07-3076)

Fig. 6: Compilation of Atlantic bottom water [CO_3^{2-}] reconstructions based on epibenthic foraminiferal B/Ca for the time interval MIS 5 to MIS 3 (Table 1). (a) Water isotope variations ($\delta^{18}O$) in the Greenland NGRIP ice core (NGRIP Members, 2004) on the AICC2012 ice age scale (Veres et al., 2013; grey) and atmospheric CO_2 concentrations (Bereiter et al., 2015; blue). Bottom water [CO_3^{2-}] reconstruction obtained in sediment cores (b) PS1243 (this study) and MD95-2039 (Yu et al., 2023) to aid a comparison on (multi-)millennial-scale timescales (error bar indicates the mean 1σ-uncertainty of $[CO_3^{2-}]_{down\text{-}core}$=9.3 µmol/kg in PS1243), (c) for North Atlantic sites MD01-2446 (Yu et al., 2016), Site U1308 (Chalk et al., 2019), Site U1313 (Chalk et al., 2019) and ODP Site 980 (Chalk et al., 2019), (d) for tropical Atlantic records at ODP Site 999 (Chalk et al., 2019), VM28-122 (Yu et al., 2010), EW9209-2JPC (Yu et al., 2016), RC16-59 (Broecker et al., 2015), GeoB1115-3, GeoB1118-3 and GeoB1117-2 (Raitzsch et al., 2011; following [CO_3^{2-}] calculations in Yu et al., 2016), and (e) for South Atlantic sites RC13-229 (Yu et al., 2016) and RC13-228 (Yu et al., 2016), MD07-3076 (Gottschalk et al., 2015) and TN057-21 (Yu et al., 2016). The map shows the locations of all cores in the Atlantic Ocean with core number referring to Table 1. Boxes at the top indicate marine isotope stages (MIS) following Lisiecki and Raymo (2005) and marine isotope substages (MIS 5e–5a) according to Railsback et al. (2015). Blue bars and numbers indicate Heinrich stadials (HS) following Capron et al. (2021). The onset of MIS 5e (*sensu stricto*) was defined in the study core after Bauch et al. (2012) as the end of ice-rafted detritus input following MIS 6.

5. Discussion

5.1 Marine Isotope Stage 5e

Despite similar mean $CO_{2,atm}$ levels (Bereiter et al., 2015) and a similar mean NADW export strength (Böhm et al., 2015) during MIS 5e and the Holocene, bottom water [CO_3^{2-}] in Norwegian Sea core PS1243 show a slight, yet statistically significant, elevation during MIS 5e compared to the Holocene (Figs. 4, 5). This is accompanied by lower surface ocean productivity at core site PS1243 during MIS 5e compared to the Holocene (Thibodeau et al., 2017), which would have resulted in lower surface water (i.e., preformed) [CO_3^{2-}] during MIS 5e. Because foraminiferal tests in core PS1243 were slightly better preserved during MIS 5e compared to the Holocene (Henrich et al., 1998, 2002; Helmke and Bauch, 2002), different contributions of alkalinity and [CO_3^{2-}] supply due to $CaCO_3$ dissolution at the bottom cannot explain the slight Holocene-versus-MIS 5e bottom water [CO_3^{2-}] offset. In addition, lower-than-Holocene aqueous CO_2 ($CO_{2,aq}$) values in the southern Norwegian sea (Ezat et al., 2017b) at the gateway of inflowing Atlantic surface waters into the Nordic Seas suggest increased preformed [CO_3^{2-}] of inflowing North Atlantic (sub-)surface waters that was likely predominantly driven by higher ocean temperatures of North Atlantic surface waters during MIS 5e (i.e., lowered solubility-driven CO_2 uptake; e.g., Bauch et al., 2012; Rodrigues et al., 2017). Indeed, *C. wuellerstorfi* $\delta^{13}C$ and [CO_3^{2-}] values in MIS 5e deviate from Holocene values on a $\delta^{13}C$-[CO_3^{2-}]-cross plot along vectors indicating higher temperatures and CO_2 evasion (Fig. 5; e.g., Yu et al., 2008), supporting a continuous and efficient transport of the pre-formed surface ocean [CO_3^{2-}] signal to depth. We therefore argue that our new bottom water [CO_3^{2-}] record reflects continued, if not strengthened, Nordic Seas convection during MIS 5e on a multi-millennial timescale.

The surface of the Nordic Seas was reconstructed to be colder during MIS 5e than during the Holocene likely due to a reduced heat supply from the Atlantic Ocean to the surface and/or deeper Atlantic water inflow (e.g., Bauch et al., 2012). We argue that along with brine expulsion during an expanded winter sea ice growth (Bauch et al., 2011, 2012; Bauch and Erlenkeuser, 2008) this led to persistent convection in the Norwegian Sea and the continuous supply of well-ventilated water masses to depth during MIS 5e. However, additional impacts on Nordic Seas surface ocean buoyancy may have arisen from the import

of Arctic buoyancy anomalies (likely related to enhanced summer sea-ice melting in the Arctic Ocean) during MIS 5e (Otto-Bliesner et al., 2006, CAPE Last Interglacial Project Members, 2006; Ezat et al., 2024). There are also multiple lines of evidence for prolonged meltwater supply from remnant MIS 6 ice sheets surrounding the Nordic Seas which extended far into MIS 5e (Bauch et al., 2011, 2012) that may have been linked with centennial- to sub-millennial-scale disruptions in NADW formation (e.g. Galaasen et al., 2014). Our new bottom water [CO_3^{2-}] data suggest that these additional influences on Nordic Seas surface ocean buoyancy did not hamper deep convection in the Norwegian Sea beyond several centuries or very few millennia. Indeed, modelling studies forced by various future $CO_{2,atm}$ scenarios suggest a weakening of the AMOC during the first century and a decline in overturning in the Nordic Seas until ~2050 that is followed by an AMOC recovery to the initial or an even stronger state (depending on the model; Bonan et al., 2022) and a strengthening of overturning in the Nordic Seas (Årthun et al., 2023). This is consistent with our observation of persistent overturning in the Norwegian Sea during MIS 5e that might have been slightly stronger than during the Holocene. The simulations suggest that stronger salinity- and temperature gradients between high- and mid-latitudes affected the transformation of surface waters into dense waters and thereby maintain active and strong overturning circulation both in the Nordic Seas and the Atlantic Ocean under warmer-than-present climate scenarios (Bonan et al., 2022; Årthun et al., 2023). Considering the global MIS 5e as a warmer-than-present (possible future) climate scenario, our data bear witness to a high resilience and/or fast recovery of Nordic Seas overturning circulation to warmer surface conditions in the North Atlantic (e.g., Bauch and Kandiano, 2007), delayed warming in the Nordic Seas (e.g., Bauch et al., 2011, 2012), changes in surface ocean buoyancy forcing through meltwater supply from surrounding ice sheets (e.g., Bauch et al., 2011) and sea ice reduction in the Arctic Ocean during MIS 5e (e.g., Otto-Bliesner et al., 2006, CAPE Last Interglacial Project Members, 2006) that likely had a stabilising effect on the AMOC overall (Bonan et al., 2022; Årthun et al., 2023).

Mean bottom water [CO_3^{2-}] during MIS 5e in Norwegian Sea core PS1243 is higher or similar to bottom water [CO_3^{2-}] in the North Atlantic Ocean (Fig. 6), supporting the representation of our bottom water [CO_3^{2-}] record as one [CO_3^{2-}] endmember of northern-component waters in the North Atlantic. Our compiled records further suggest that overflows from the Nordic Seas into the eastern North Atlantic (ODP Site 980) persisted during MIS 5e, potentially facilitated by active ISOW (Crocket et al., 2011). Given a substantial and continuous production of DSOW during MIS 5e (Hillaire-Marcel et al., 2001), despite reductions in Labrador Sea Water formation or even its absence (Cottet-Puinel et al., 2004; Winsor et al., 2012), our data indicate that NSSW remains an important contributor to NADW on timescales of (multiple) millennia during this period.

5.2 Marine Isotope Stage 5e to 5a

Reconstructed bottom water [CO_3^{2-}] in the deep Norwegian Sea remain constant across the MIS 5e/d transition, despite a ~40 ppm decline in $CO_{2,atm}$ (Fig. 4; Bereiter et al., 2015). In addition, CO_2 uptake in the upper ocean at the Iceland-Scotland-Ridge increased at that time as evidenced by a rise in $CO_{2,aq}$ concentrations approaching near-equilibrium levels under constant nutrient conditions and decreasing (sub-)SST (Fig. 7; Ezat et al., 2016, 2017b). A $CO_{2,atm}$ drop would operate to increase preformed [CO_3^{2-}] levels in the Nordic Seas, while upper-ocean CO_2 uptake and -cooling at the MIS 5e/d transition acts to

lower preformed [CO_3^{2-}] levels. The latter is supported by increasing *N. pachyderma* $\delta^{18}O$ levels in core PS1243 and a decline in reconstructed (sub-)SST in the southern Norwegian Sea at the MIS 5e/d boundary (Fig. 7; Rasmussen et al., 2003; Ezat et al., 2016). In addition, thermodynamically controlled $\delta^{13}C$ fractionation between the atmosphere and the surface ocean operates to increase DIC $\delta^{13}C$ during cooling (Lynch-Stieglitz et al., 1995), which is reflected in a rise of *N. pachyderma*-, and consequently also *C. wuellerstorfi*, $\delta^{13}C$ levels at our core site (Fig. 7). Based on *C. wuellerstorfi* B/Ca-derived bottom water [CO_3^{2-}] at the Iberian margin, Yu et al. (2023) argued for a strong solubility-driven uptake of CO_2 in the North Atlantic and Nordic Seas because of upper-ocean cooling at the MIS 5e/d transition (i.e., Greenland stadial 26 specifically), which is consistent with our inference from core PS1243. However, we argue that decreasing $CO_{2,atm}$ levels caused a rise in surface water [CO_3^{2-}] in the Atlantic Ocean (i.e., source water [CO_3^{2-}]) that acted to raise preformed [CO_3^{2-}] in the study area through northward transport. This increase in preformed [CO_3^{2-}] was then counterbalanced by cooling-induced increase in CO_2 solubility in the Nordic Seas leading to nominally unchanged preformed [CO_3^{2-}] of surface waters at our study site. Consequently, enhanced deep-water formation, along with potentially minor contributions from changes in sea ice (through $CO_{2,aq}$ enrichment in brines; Rysgaard et al., 2009), surface ocean productivity (influencing surface ocean [CO_2]), and carbonate dissolution at the sea floor (releasing alkalinity at depth), maintained constant bottom water [CO_3^{2-}] in the deep Norwegian Sea during the MIS 5d/e transition (Fig. 7). This is consistent with PS1243 *C. wuellerstorfi* $\delta^{13}C$ and [CO_3^{2-}] data during MIS 5e and MIS 5d that are primarily separated from each other in $\delta^{13}C$-[CO_3^{2-}]-space along the temperature vector influencing DIC $\delta^{13}C$ levels only, with different effects on air-sea CO_2 exchange cancelling each other out (Fig. 5). Overall, our bottom water [CO_3^{2-}] data suggest continuous deep-water formation in the Nordic Seas at the MIS 5e/d transition, and hence the transformation of lighter upper-ocean waters to dense water masses and their transport to depth in the Norwegian Sea (Figs. 4, 7).

Bottom waters in the deep Norwegian Sea during MIS 5 are generally characterised by higher-than-Holocene [CO_3^{2-}] with a marked rise starting after HS10 at 103 ka BP (Fig. 6). This suggests overall persistent deep-water formation in the Nordic Seas during that time, which is supported by increased abundances of the pteropod *Limacina spp.* in PS1243 sediments from MIS 5c to 5a (Fig. 4). The appearance of *Limacina* spp. may indicate a deepening of the aragonite compensation depth of at least 700 m from its modern position in the Norwegian Sea (~2000 m; Lauvset et al., 2022) and a shift in the aragonite saturation state from present-day levels of Ω_A=0.8 to above 1.0 at core site PS1243 (Fig. 1b). These changes were likely primarily driven by enhanced or persistent deep Norwegian Sea convection, with possible influences from changes in the export production of *Limacina* spp. shells (Fig. 4), which might have provided a source of alkalinity to bottom waters through (partial) aragonite dissolution, acting to raise bottom water [CO_3^{2-}] (Sulpis et al., 2022). Higher-than-Holocene bottom water [CO_3^{2-}] between 46–40 ka BP and increased preservation of *Limacina* spp. throughout MIS 3 recorded in PS1243 sediments support the notion of persistent deep Norwegian Sea convection (Fig. 4). Overall, we argue that despite possible temporal changes in pteropod export fluxes and seafloor aragonite dissolution rates in the Norwegian Sea over the last glacial cycle that are largely unknown, increased preservation of aragonite shells during MIS 5c to 5a strongly supports sustained deep-water formation and ventilation during that time. However, assessing the influence of potential changes in pteropod fluxes and dissolution rates in the water

column (e.g., supralysoclinal) and in bottom waters (e.g., below the lysocline) on [CO_3^{2-}] in the Nordic Seas and how this might have affected the Atlantic Ocean via dense overflows requires further investigation.

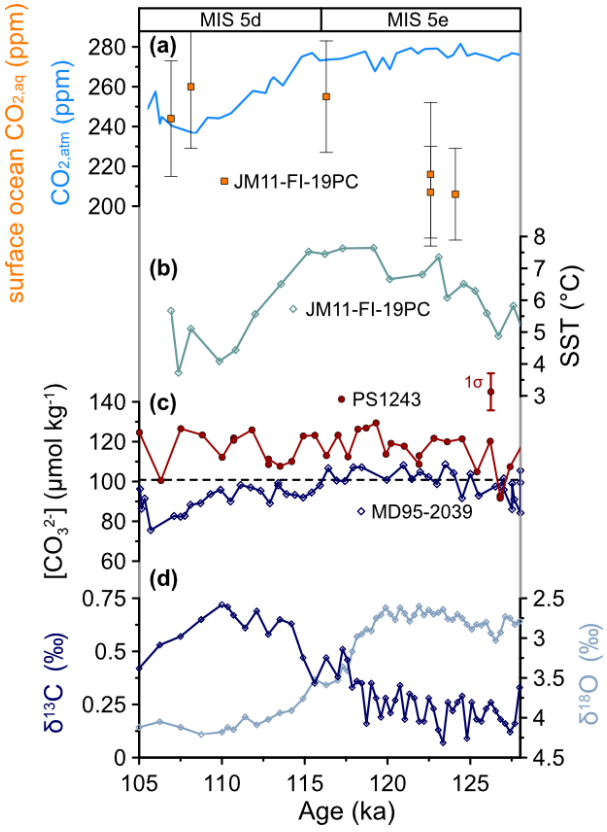

Fig. 7: Comparison of North Atlantic and Norwegian Sea bottom water [CO_3^{2-}] estimates to surface water parameters reconstructed for the MIS 5e-to-5d transition. (a) Atmospheric CO_2 ($CO_{2,atm}$) concentration (Bereiter et al., 2015; blue) and reconstructed surface ocean dissolved, aqueous CO_2 levels ($CO_{2,aq}$) corrected by -40 ppm for the calcification depth of *N. pachyderma* in southern Norwegian Sea core JM11-FI-19PC (Ezat et al., 2017b; orange). (b) *N. pachyderma* Mg/Ca-based sea surface temperatures (SST) in core JM11-FI-19PC (Ezat et al., 2016). (c) Bottom water [CO_3^{2-}] record of PS1243 (this study, red) and MD95-2039 (Yu et al., 2023; blue). Error bar indicates the mean 1σ-uncertainty of [CO_3^{2-}]$_{down\text{-}core}$=9.3 µmol/kg in PS1243. (d) *N. pachyderma* $\delta^{18}O$ (dark blue) and $\delta^{13}C$ (light blue) in core PS1243 (Bauch et al., 2012). Boxes at the top indicate marine isotope stages (MIS) following Lisiecki and Raymo (2005) and marine isotope substages (MIS 5a–5e) according to Railsback et al. (2015). The onset of MIS 5e (*sensu stricto*) was defined in the study core after Bauch et al. (2012) as the end of ice-rafted detritus input following MIS 6.

At face value, bottom water [CO_3^{2-}] in the deep Norwegian Sea (PS1243, this study) and the deep Iberian Margin site (MD95-2039, Yu et al., 2023) tend to anti-correlate on millennial timescales during MIS 5, with higher [CO_3^{2-}] in the deep Norwegian Sea and lower [CO_3^{2-}] at the Iberian margin during HS (Figs. 4, 6). However, this observation may be biased by bioturbational smoothing of the signal given the low sedimentation rate of our study core, which depends on the mixed layer depth (MLD), abundances of foraminifera (as the proxy carrier) and their variations as well as the magnitude of the proxy signal (e.g., Anderson, 2001; Trauth, 2013). Therefore, we employ sensitivity tests with the simple sediment mixing model of Trauth (2013)

to assess the effects of bioturbational mixing on our [CO_3^{2-}] for MLD ranging between 5 and 15 cm and for a hypothetical (i.e., pre-mixing) 30 µmol/kg-decline and a hypothetical 30 µmol/kg-increase in bottom water [CO_3^{2-}] during HS8 and 9 (Fig. 8). Out of the eight tested scenarios, we find that our proxy-based [CO_3^{2-}] estimates are consistent with a [CO_3^{2-}] increase during HS8 and 9 (Fig. 8) overprinted by bioturbation with an MLD of 7 cm that is in fact close to the global mean of ~6 cm (Teal et al., 2008). Therefore, we cannot exclude that the mismatch between bottom water [CO_3^{2-}] in cores PS1243 and MD95-2039 during HS in MIS 5 is a true signal (Figs. 6, 8). This in turn may hint at continued deep-water formation in the Nordic Seas and a southern outflow in the Atlantic Ocean likely via the Denmark Strait during HS of MIS 5, which could have caused a zonal gradient in bottom water [CO_3^{2-}] between the deep western and eastern North Atlantic, and hence between PS1243 and MD95-2039. However, unravelling NSSW [CO_3^{2-}] variability, its dispersal in the Atlantic Ocean and its influence on whole-Atlantic Ocean ventilation and CO_2 release during stadial-interstadial cycles (Yu et al., 2023) requires high-resolution bottom water [CO_3^{2-}] records from high-sedimentation sites in the Nordic Seas as well as from deep Atlantic sites (e.g., from the deep western basin of the Atlantic Ocean).

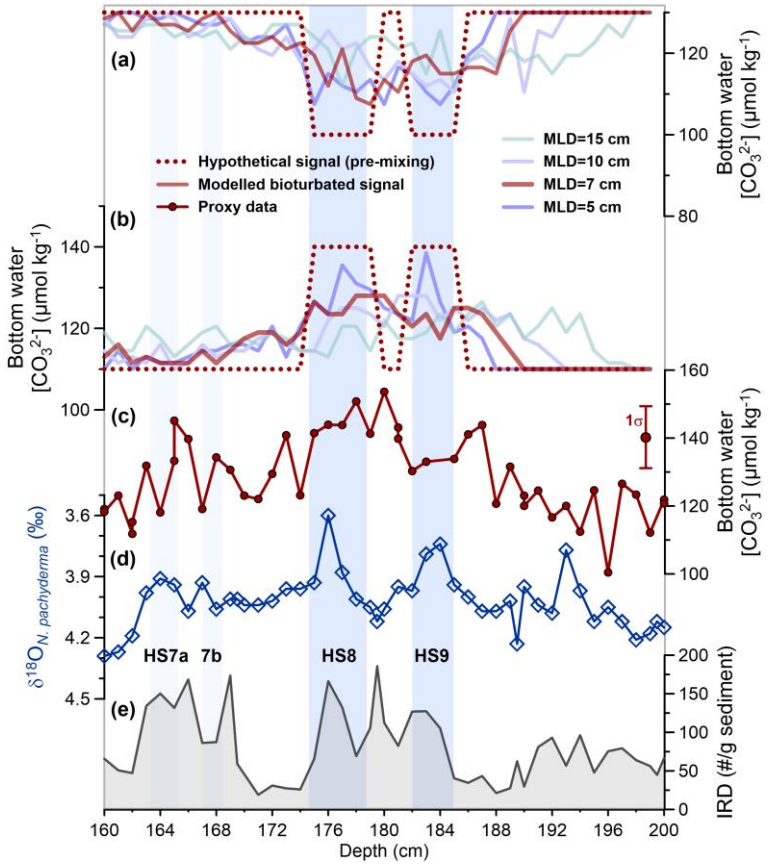

Fig. 8: Effects of bioturbational mixing on millennial-scale bottom water [CO_3^{2-}] variations in core PS1243 during Heinrich Stadial (HS) 8 and 9 as a function of the mixed layer depth (MLD) based on the sediment-mixing-model of Trauth (2013) shown against

core depth. Modelled bioturbated [CO_3^{2-}] signal (solid lines) for (a) a hypothetical 30 µmol/kg-decline (this magnitude matches observations in Yu et al. (2023)) and (b) a hypothetical 30 µmol/kg-increase in bottom water [CO_3^{2-}] during HS8 and 9 (stippled lines) for a MLD of 5 cm (purple), 7 cm (red), 10 cm (light purple) and 15 cm (light green). (c) Bottom water [CO_3^{2-}] estimates (this study), (d) *N. pachyderma* $\delta^{18}O$ variations and (e) ice-rafted detritus (IRD) abundances in PS1243 (Bauch et al., 2012). Our sediment-mixing model runs do neither consider changes in the abundance of *C. wuellerstorfi* that the reconstructions of [CO_3^{2-}] are based on nor [CO_3^{2-}] changes on glacial-interglacial timescales. Blue bars and numbers indicate Heinrich stadials (HS) HS7a, 7b, 8 and 9 following Capron et al. (2021).

5.3 Marine Isotope Stage 5a to 4

At the MIS 5a-to-4 transition, Yu et al. (2016) found a marked decrease in bottom water [CO_3^{2-}] by ~25 µmol/kg in Atlantic Ocean cores below 3 km water depth (Fig. 6). This trend, however, contrasts with high bottom water [CO_3^{2-}] at ODP Site 999 and in core VM28-122 from the Caribbean Basin at 1.8 km water depth, with ODP Site 980 in the Northeast Atlantic at 2.2 km water depth (Broecker et al., 2015; Chalk et al., 2019) as well as with core PS1243 in the Norwegian Sea at 2.7 km water depth (this study, Fig. 6). We argue based on our new data that, despite possible changes in preformed [CO_3^{2-}] due to lower $CO_{2,atm}$ levels during MIS 4, the Nordic Seas were characterised by continuous deep convection at that time. In addition, the formation of deep waters in the Nordic Seas and overflows to the Atlantic basin likely contributed to GNAIW that was in turn suggested to be dominantly influenced by a shallow convection cell south of Iceland (Broecker et al., 2015; Chalk et al., 2019). However, similar trends in bottom water [CO_3^{2-}] in the deep Norwegian Sea and in the intermediate Atlantic Ocean at ODP Sites 980 and 999 and in core VM28-122 (Broecker et al., 2015; Chalk et al., 2019) emphasises strong contributions of well-ventilated, high-[CO_3^{2-}] NSSW to GNAIW via high-density overflows to the intermediate North Atlantic during MIS 4. This aligns with findings of strong (nearly modern-like) AMOC intensity in the western North Atlantic during MIS 4 (Böhm et al., 2015) and an increased presence of northern-component waters in the Atlantic Ocean at that time (Pöppelmeier et al., 2021).

The widespread decline in deep Atlantic [CO_3^{2-}] below 3 km water depth was linked with a rise in respired carbon levels and/or a greater admixture of northward expanded, [CO_3^{2-}]-low southern-sourced waters (SSW; Yu et al., 2016). The glacial northward expansion of SSW in the Atlantic Ocean was postulated to have driven a marked geochemical- and density separation between Glacial Antarctic Bottom Water (GAABW) and GNAIW at 2–3 km water depth (e.g., Adkins, 2013; Yu et al., 2016) and a concomitant drop in $CO_{2,atm}$ levels through an increase in deep Atlantic respired carbon storage (Yu et al., 2016). However, while the overflow intensity east of Iceland via ISOW might have decreased during MIS 4, possibly triggered by a glacial deeper (i.e., subsurface) inflow of ASW (Bauch et al., 2001; Nørgaard-Pedersen et al., 2003; Rasmussen and Thomsen, 2009; Ezat et al., 2021), the expansion of NSSW-influenced GNAIW was likely focussed in the western North Atlantic. This is consistent with a stronger influence of SSW in the eastern Atlantic basin compared to the Northwest Atlantic Ocean (Chalk et al., 2019). The contribution of high-[CO_3^{2-}] (low-[$CO_{2,aq}$]) NSSW to the Northwest Atlantic would have limited the capacity of the Atlantic Ocean to store carbon during MIS 4 that likely was mostly stemmed in the eastern basin. Due to the lack of bottom water [CO_3^{2-}] reconstructions below 3 km water depth in the western North Atlantic, contributions of NSSW overflows to the abyssal Northwest Atlantic during MIS 4, as postulated previously for the LGM (Keigwin and Swift, 2017; Blaser et al., 2020; Larkin et al., 2022), can neither be identified nor ruled out. Overall, the zonal and meridional

extent of high-[CO_3^{2-}], NSSW-influenced GNAIW in the western Atlantic Ocean remains poorly constrained, making a quantification of the impact of continuous NSSW contributions to the Atlantic and their role in Atlantic Ocean respired carbon levels difficult.

5.4 Comparison between Marine Isotope Stage 4 and 2

Although core PS1243 lacks bottom water [CO_3^{2-}] estimates for MIS 2, our compilation of Atlantic Ocean bottom water [CO_3^{2-}] records indicate that the Atlantic water mass structure and its [CO_3^{2-}] characteristics during MIS 2 and MIS 4 share strong similarity, with diverging shallow Atlantic and deep Atlantic/Nordic Seas [CO_3^{2-}] records at the inception of MIS 4 (Fig. 9, Table 1; Yu et al., 2008, 2020; Broecker et al., 2015; Chalk et al., 2019). We therefore argue that fundamental characteristics of the North Atlantic and the Nordic Seas were similar during MIS 2 and MIS 4, including a sustained, subsurface inflow of warm, saline Atlantic waters (Bauch et al., 2001, 2012; Kandiano and Bauch, 2002; Nørgaard-Pedersen et al., 2003; Rasmussen and Thomsen 2009; Ezat et al., 2014, 2021), continuous overturning circulation and dense water formation in the Nordic Seas (e.g. Veum et al., 1992; Weinelt et al., 1996; Larkin et al., 2022), and persistent NSSW overflow into the western glacial North Atlantic and its marked contribution to GNAIW and possibly abyssal waters (i.e., glacial NADW (GNADW); Veum et al., 1992; Millo et al., 2006; Yu et al., 2008; Crocket et al., 2011; Crocker et al., 2016; Ezat et al., 2017a, 2021; Larkin et al., 2022). Additionally, bottom water (i.e., *C. wuellerstorfi*) $\delta^{13}C$ and [CO_3^{2-}] during MIS 4 in our Norwegian Sea core PS1243 align, within uncertainties, reconstructed endmember values of GNAIW during MIS 2 ($\delta^{13}C$=1.5‰ VPDB, [CO_3^{2-}]=~140 µmol/kg; Fig. 5, Yu et al., 2020). Continued dense water formation in the Nordic Seas during MIS 2 and MIS 4 is also consistent with high *C. wuellerstorfi* $\delta^{13}C$ values in core PS1243 (Fig. 4), good and in parts excellent carbonate preservation in the Nordic Seas during glacials (Henrich et al., 1998, 2002; Helmke and Bauch, 2002) and low subsurface $CO_{2,aq}$ levels in the Norwegian Sea at those times (Ezat et al., 2017b). Furthermore, there is increasing evidence of northern-sourced deep waters in the Atlantic during the LGM (Hoffmann et al., 2013; Howe et al., 2016; Keigwin and Swift 2017; Oppo et al., 2018; Pöppelmeier et al., 2021) likely fed by continuous bottom water sourcing from the Nordic Seas (Blaser et al., 2020; Larkin et al., 2022). This was also emphasised for MIS 4 by Pöppelmeier et al. (2021) who found a rise in the proportion of northern-component waters in the equatorial and Northeast Atlantic by additional ~15%, which supports our bottom water [CO_3^{2-}]-based inferences from core PS1243.

Sustained dense water formation and ventilation of Nordic Seas deep waters during MIS 2 and MIS 4 were likely facilitated by a combination of saline Atlantic water subsurface inflow (Bauch et al., 2001) and a contribution of brines from sea-ice formation (Veum et al., 1992; Dokken and Jansen, 1999; Bauch and Bauch, 2001). Deep convection was further promoted through the formation of polynyas driven by strong catabatic winds downflowing from proximal ice sheets and shelves (e.g., Bauch et al., 2001; Knies et al., 2018). There remain, however, two contrasting views on the impact of dense NSSW water on the Atlantic Ocean, either as a shallow contribution to GNAIW (e.g., Yu et al., 2008, 2020) or as a dense contribution to abyssal waters resulting in GNADW (e.g., Millo et al., 2006; Howe et al., 2016; Keigwin and Swift, 2017; Ezat et al., 2019).

Irrespective of the exact nature of an NSSW contribution to the North Atlantic Ocean that is ultimately density-dependent, we provide evidence for continuous formation of well-ventilated, high-[CO_3^{2-}] NSSW in the Nordic Seas during MIS 4 that likely advected into the northwest Atlantic Ocean via Denmark Strait overflows (Millo et al., 2006; Ezat et al., 2021). Yet, epibenthic foraminiferal B/Ca-derived [CO_3^{2-}] records in the western North Atlantic are limited but urgently needed to estimate the Atlantic Ocean volume influenced by well-ventilated NSSW and to understand the role of the North Atlantic in glacial deep-sea respired CO_2 storage during MIS 2 and MIS 4.

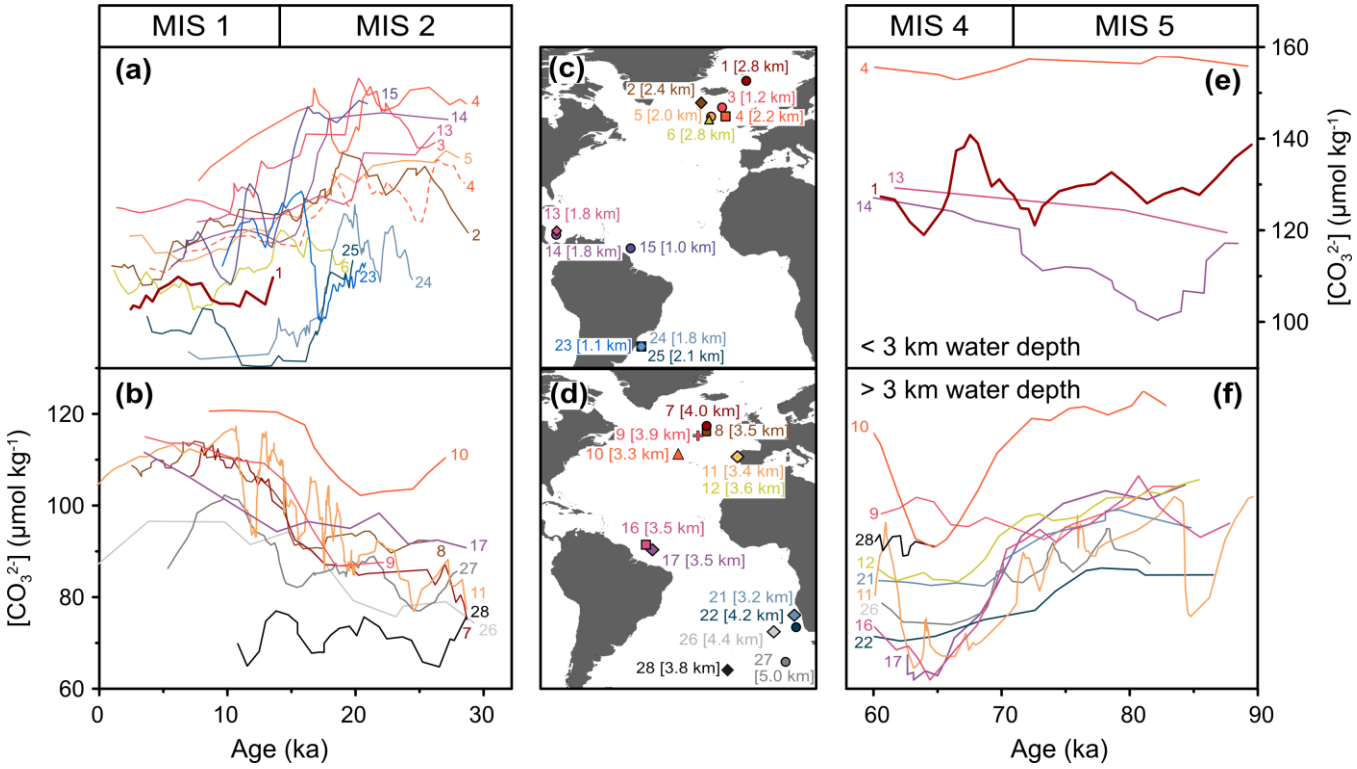

Fig. 9: Compilation of Atlantic bottom water [CO_3^{2-}] reconstructions (five point-running means) for the time intervals a, b) MIS 2 to MIS 1 (i.e., the last deglaciation) and e, f) MIS 5a to MIS 4 (i.e., the last glacial inception) (numbers at core locations and timeseries refer to core locations given in Table 1). c, d) Core locations of epibenthic foraminiferal B/Ca-based [CO_3^{2-}] reconstructions from the Atlantic Ocean and the Nordic Seas (numbers at core locations refer to metadata given in Table 1 and numbers in brackets highlight the water depth at the core sites), with colours equivalent to those shown at the onset (a, b) and end (e, f) of the reconstructed bottom water [CO_3^{2-}] records. The bottom water [CO_3^{2-}] record of ODP Site 980 (with label number 4) in a) is shown as solid line following Chalk et al. (2019) and as dashed orange line following the record of Crocker et al. (2016). *C. wuellerstorfi* B/Ca from Crocker et al. (2016) was converted into [CO_3^{2-}] using the calibration applied in section 3.3 (Yu and Elderfield, 2007) and using the core-top [CO_3^{2-}] value (119 µmol/kg) reported by Chalk et al. (2019). Upper and lower panels show core sites shallower and deeper than 3 km water depth, respectively. Boxes at the top indicate marine isotope stages (MIS) following Lisiecki and Raymo (2005) and marine isotope substages (MIS 5a) according to Railsback et al. (2015).

6. Conclusion

Using sediment core PS1243 from the deep Norwegian basin, we reconstructed bottom water [CO_3^{2-}] inferred from *C. wuellerstorfi* B/Ca ratios. We have further increased the resolution of the existing *C. wuellerstorfi* $\delta^{13}C$ record for the past

130 ka for the study core and show an unprecedented data set of continuous aragonite preservation in the Norwegian Sea based on the pteropod *Limacina* spp. for much of the last glacial cycle (~98–31 ka BP). The main focus of the study is to assess glacial-interglacial changes in the overturning strength of the Nordic Seas. An Atlantic Ocean compilation of existing bottom water [CO_3^{2-}] records over the last glacial cycle further allowed a comparison with our new bottom water [CO_3^{2-}] estimates to evaluate potential effects of Nordic Seas convection and dense-water overflows across the Greenland-Scotland Ridge on the chemical water mass structure and respired carbon storage in the Atlantic Ocean.

Bottom water [CO_3^{2-}] in the deep Nordic Seas during MIS 5e are similar (within uncertainties) to published bottom water [CO_3^{2-}] records from the Atlantic Ocean, suggesting that our PS1243 [CO_3^{2-}] record serves as the [CO_3^{2-}] endmember of Nordic Seas-sourced deep waters, and represents one important endmember of northern-component waters in the North Atlantic during that time. The bottom water [CO_3^{2-}] data during MIS 5e further indicate overall persistent deep-water formation in the Norwegian Sea, despite the possibility of centennial- or sub-millennial-scale phases of weakening and despite a generally warmer North Atlantic and cooler upper Nordic Seas when compared to the Holocene. Such a scenario is consistent with numerical model simulations that attest overturning in the Nordic Seas and the Atlantic Ocean a high resilience towards future climate forcing on longer timescales and might therefore testify a stabilising effect of continued Nordic Seas convection and associated overflows on Atlantic overturning (Bonan et al., 2022; Årthun et al., 2023).

The MIS 5d/e transition was characterised by constant, yet high bottom water [CO_3^{2-}] in the deep Norwegian Sea. We argue that this primarily reflects persistent deep-water formation in the Nordic Seas and a shift in preformed [CO_3^{2-}] levels driven by declining $CO_{2,atm}$ levels that is compensated by CO_2 solubility-driven changes in preformed [CO_3^{2-}] due to upper-ocean cooling. Generally higher-than-Holocene [CO_3^{2-}] throughout MIS 5 and the dominant occurrence of the pteropod *Limacina* spp. in MIS 5c-to-a sediments indicate a marked deepening of the aragonite compensation depth by at least 700 m in the Norwegian Sea, albeit effects from changes in pteropod export fluxes cannot be excluded. This bears witness to persistent dense-water formation and deep-water ventilation in the Nordic Seas throughout MIS 5.

The MIS 5a to 4 transition is marked by a divergence of shallow Atlantic Ocean- and deep Norwegian Sea [CO_3^{2-}] from Atlantic [CO_3^{2-}] records deeper than 3 km water depth, which is reminiscent of similar trends during the LGM (e.g., Yu et al., 2020). This suggests a persistent (subsurface) inflow of Atlantic waters into the Nordic Seas, continuous glacial deep-water formation in the Nordic Seas and sustained contributions of NSSW to the Atlantic Ocean via dense-water overflows during MIS 4. Whether this also applies to stadial intervals (e.g., HS within MIS 5) requires further testing based on high resolution [CO_3^{2-}] records from high-accumulation sites in the Nordic Seas and the deep western Atlantic Ocean.

Overall, our study puts new constraints on the [CO_3^{2-}] end-member composition of deep waters emerging from the Nordic Seas on multi-millennial timescales during MIS 5 and MIS 4, and highlights the persistent formation of well-ventilated deep waters in the Norwegian Sea in spite of contrasting changes in surface ocean properties during these climatically variable times. However, additional bottom water [CO_3^{2-}] reconstructions, primarily from the deep western Atlantic Ocean and the Greenland or Iceland Sea, are needed to further constrain the nature of Nordic Seas overturning as well as the extent and impact of NSSW on the water mass structure, overturning strength, and ultimately the carbon storage capacity of the Atlantic Ocean

throughout the last glacial cycle to fully understand the role of the Atlantic Ocean and the Nordic Seas in Atlantic overturning dynamics and $CO_{2,atm}$ variations.

Code and data availability: The map and transects of the study area (Figure 1) were made with Ocean Data View (Schlitzer, 2022) version 5.6.5, available at https://odv.awi.de (last access: 30 July 2024). Data from this study are openly available from the PANGAEA database at https://doi.org/10.1594/PANGAEA.973144 (Stobbe et al., 2025).

Author contributions: TBS: Conceptualisation, Investigation, Methodology, Visualisation, Writing – original draft preparation. HAB: Conceptualisation, Resources (stable isotope analysis, samples, pteropods), Writing – reviewing & editing. DAF: Resources (Laboratory infrastructure), Data curation, Writing – reviewing & editing. JY: Writing – reviewing & editing. JG: Conceptualisation, Methodology, Visualisation, Funding acquisition (Trace element analysis), Project administration, Resources (Laboratory infrastructure), Writing – original draft preparation, reviewing & editing.

Competing interests: The contact author has declared that none of the authors has any competing interests.

Acknowledgements: We thank U. Westernströer and K. Bremer for their assistance with laboratory work, and S. Kraft for picking and weighing pteropods. We are also grateful to M.M. Ezat for valuable insights into foraminiferal trace element analyses in the study area.

References

Adkins, J. F.: The role of deep ocean circulation in setting glacial climates, Paleoceanography, 28, 539–561, https://doi.org/10.1002/palo.20046, 2013.

Anderson, D. M.: Attenuation of Millennial-Scale Events by Bioturbation in Marine Sediments, Paleoceanography, 16, 352–357, https://doi.org/10.1029/2000PA000530, 2001.

Årthun, M., Asbjørnsen, H., Chafik, L., Johnson, H. L., and Våge, K.: Future strengthening of the Nordic Seas overturning circulation, Nat. Commun., 14, 2065, https://doi.org/10.1038/s41467-023-37846-6, 2023.

Barker, S., Greaves, M., and Elderfield, H.: A study of cleaning procedures used for foraminiferal Mg/Ca paleothermometry, Geochem. Geophy. Geosy., 4, https://doi.org/10.1029/2003GC000559, 2003.

Bauch, D. and Bauch, H. A.: Last glacial benthic foraminiferal $\delta^{18}O$ anomalies in the polar North Atlantic: A modern analogue evaluation, J. Geophys. Res., 106, 9135–9143, https://doi.org/10.1029/1999JC000164, 2001.

Bauch, H. A. and Weinelt, M. S.: Surface water changes in the Norwegian sea during last deglacial and holocene times, Quaternary Sci. Rev., 16, 1115–1124, https://doi.org/10.1016/S0277-3791(96)00075-3, 1997.

Bauch, H. A. and Erlenkeuser, H.: Interpreting Glacial-Interglacial Changes in Ice Volume and Climate From Subarctic Deep Water Foraminiferal δ18O, in: Earth's Climate and Orbital Eccentricity: The Marine Isotope Stage 11 Question, Geoph. Monog. Series 137, edited by: Droxler, L. H., Poore, A. W., and Burckle, R. Z., American Geophysical Union, Washington, D.C., 87–102, 2003.

Bauch, H. A., and Kandiano, E. S.: Evidence for early warming and cooling in North Atlantic surface waters during the last interglacial, Paleoceanography, 22, PA1201, doi:10.1029/2005PA001252, 2007.

Bauch, H. A. and Erlenkeuser, H.: "critical" climatic evaluation of last interglacial (MIS 5e) records from the Norwegian Sea, Polar Res., 27, 135–151, https://doi.org/10.3402/polar.v27i2.6172, 2008.

Bauch, H. A., Erlenkeuser, H., Spielhagen, R. F., Struck, U., Matthiessen, J., Thiede, J., and Heinemeier, J.: A multiproxy reconstruction of the evolution of deep and surface waters in the subarctic Nordic seas over the last 30,000 yr, Quaternary Sci. Rev., 20, 659–678, https://doi.org/10.1016/S0277-3791(00)00098-6, 2001.

Bauch, H. A., Kandiano, E.S., Helmke, J.P., Andersen, N., Rosell-Mele, A., and Erlenkeuser, H.: Climatic bisection of the last interglacial warm period in the Polar North Atlantic, Quaternary Sci. Rev., 30, 1813–1818, https://doi.org/10.1016/j.quascirev.2011.05.012, 2011.

Bauch, H. A., Kandiano, E. S., and Helmke, J. P.: Contrasting ocean changes between the subpolar and polar North Atlantic during the past 135 ka, Geophys. Res. Lett., 39, https://doi.org/10.1029/2012GL051800, 2012.

Bauerfeind, E., Nöthig, E.-M., Pauls, B., Kraft, A., Beszczynska-Möller, A.: Variability in pteropod sedimentation and corresponding aragonite flux at the Arctic deep-sea long-term observatory HAUSGARTEN in the eastern Fram Strait from 2000 to 2009, J. Marine Syst., 132, 95-105, https://doi.org/10.1016/j.jmarsys.2013.12.006, 2014

Bereiter, B., Lüthi, D., Siegrist, M., Schüpbach, S., Stocker, T. F., and Fischer, H.: Mode change of millennial CO_2 variability during the last glacial cycle associated with a bipolar marine carbon seesaw, Proceedings of the National Academy of Sciences of the United States of America, 109, 9755–9760, https://doi.org/10.1073/pnas.1204069109, 2012.

Bereiter, B., Eggleston, S., Schmitt, J., Nehrbass-Ahles, C., Stocker, T. F., Fischer, H., Kipfstuhl, S., and Chappellaz, J.: Revision of the EPICA Dome C CO_2 record from 800 to 600 kyr before present, Geophys. Res. Lett., 42, 542–549, https://doi.org/10.1002/2014GL061957, 2015.

Blaser, P., Gutjahr, M., Pöppelmeier, F., Frank, M., Kaboth-Bahr, S., and Lippold, J.: Labrador Sea bottom water provenance and REE exchange during the past 35,000 years, Earth Planet. Sc. Lett., 542, 116–299, https://doi.org/10.1016/j.epsl.2020.116299., 2020

Böhm, E., Lippold, J., Gutjahr, M., Frank, M., Blaser, P., Antz, B., Fohlmeister, J., Frank, N., Andersen, M. B., and Deininger, M.: Strong and deep Atlantic meridional overturning circulation during the last glacial cycle, Nature, 517, 73–76, https://doi.org/10.1038/nature14059, 2015.

Bonan, D. B., Thompson, A. F., Newsom, E. R., Sun, S., and Rugenstein, M.: Transient and equilibrium responses to the Atlantic Overturning Circulation to warming in coupled climate models: The role of temperature and salinity, J. Climate, 35, 5173–5193, https://doi.org/10.1175/JCLI-D-21-0912.1, 2022.

Boyle, E. A.: Manganese carbonate overgrowths on foraminifera tests, Geochim. Cosmochim. Ac., 47, 1815–1819, https://doi.org/10.1016/0016-7037(83)90029-7, 1983.

Boyle, E. A. and Keigwin, L.: North Atlantic thermohaline circulation during the past 20,000 years linked to high-latitude surface temperature, Nature, 330, 35–40, https://doi.org/10.1038/330035a0, 1987.

Broecker, W. S. and Clark, E.: Glacial-to-Holocene redistribution of carbonate ion in the deep sea, Science, 294, 2152–2155, https://doi.org/10.1126/science.1064171, 2001.

Broecker, W. S., Yu, J., and Putnam, A. E.: Two contributors to the glacial CO_2 decline, Earth Planet. Sc. Lett., 429, 191–196, https://doi.org/10.1016/j.epsl.2015.07.019, 2015.

CAPE-Last Interglacial Project Members: Last Interglacial Arctic warmth confirms polar amplification of climate change, Quaternary. Sci. Rev., 25, 1383–1400, https://doi.org/10.1016/j.quascirev.2006.01.033, 2006.

Capron, E., Rasmussen, S. O., Popp, T. J., Erhardt, T., Fischer, H., Landais, A., Pedro, J. B., Vettoretti, G., Grinsted, A., Gkinis, V., Vaughn, B., Svensson, A., Vinther, B. M., and White, J. W. C.: The anatomy of past abrupt warmings recorded in Greenland ice, Nat. Commun., 12, 2106, https://doi.org/10.1038/s41467-021-22241-w, 2021.

Chalk, T. B., Foster, G. L., and Wilson, P. A.: Dynamic storage of glacial CO_2 in the Atlantic Ocean revealed by boron [CO_3^{2-}] and pH records, Earth Planet. Sc. Lett., 510, 1–11, https://doi.org/10.1016/j.epsl.2018.12.022, 2019.

Clark, P. U. and Huybers, P.: Global change: Interglacial and future sea level, Nature, 462, 856–857, https://doi.org/10.1038/462856a, 2009.

Cortijo, E., Duplessy, J. C., Labeyrie, L., Leclaire, H., Duprat, J. and van Wearing, T. C. E.: Eemian cooling in the Norwegian Sea and North Atlantic Ocean preceding continental ice-sheet growth, Nature, 372, 446–449, https://doi.org/10.1038/372446a0, 1994.

Cottet-Puinel, M., Weaver, A. J., Hillaire-Marcel, C., Vernal, A. de, Clark, P. U., and Eby, M.: Variation of Labrador Sea Water formation over the Last Glacial cycle in a climate model of intermediate complexity, Quaternary Sci. Rev., 23, 449–465, https://doi.org/10.1016/S0277-3791(03)00123-9, 2004.

Crocker, A. J., Chalk, T. B., Bailey, I., Spencer, M. R., Gutjahr, M., Foster, G. L., and Wilson, P. A.: Geochemical response of the mid-depth Northeast Atlantic Ocean to freshwater input during Heinrich events 1 to 4, Quaternary Sci. Rev., 151, 236–254, https://doi.org/10.1016/j.quascirev.2016.08.035, 2016.

Crocket, K. C., Vance, D., Gutjahr, M., Foster, G. L. and Richards, D. A.: Persistent Nordic deep-water overflow to the glacial North Atlantic. *Geology,* 39, 515–518, https://doi.org/10.1130/G31677.1, 2011.

Curry, W. B. and Oppo, D. W.: Glacial water mass geometry and the distribution of $\delta^{13}C$ of ΣCO_2 in the western Atlantic Ocean, Paleoceanography, 20, https://doi.org/10.1029/2004PA001021, 2005.

Dickson, A. G. and Millero, F. J.: A comparison of the equilibrium constants for the dissociation of carbonic acid in seawater media, Deep Sea Research Part A. Oceanographic Research Papers, 34, 1733–1743, https://doi.org/10.1016/0198-0149(87)90021-5, 1987.

Dickson, A. G.: Thermodynamics of the dissociation of boric acid in synthetic seawater from 273.15 to 318.15 K, Deep Sea Research Part A. Oceanographic Research Papers, 37, 755–766, https://doi.org/10.1016/0198-0149(90)90004-F, 1990.

Dickson, R. R. and Brown, J.: The production of North Atlantic Deep Water: Sources, rates, and pathways, J. Geophys. Res., 99, 12319, https://doi.org/10.1029/94JC00530, 1994.

Dokken, T. M. and Jansen, E.: Rapid changes in the mechanism of ocean convection during the last glacial period, Nature, 401, 458–461, https://doi.org/10.1038/46753, 1999.

Ezat, M. M., Rasmussen, T. L., and Groeneveld, J.: Persistent intermediate water warming during cold stadials in the southeastern Nordic seas during the past 65 k.y, Geology, 42, 663–666, https://doi.org/10.1130/G35579.1, 2014.

Ezat, M. M., Rasmussen, T. L., and Groeneveld, J.: Reconstruction of hydrographic changes in the southern Norwegian Sea during the past 135 kyr and the impact of different foraminiferal Mg/Ca cleaning protocols, Geochem. Geophy. Geosy., 17, 3420–3436, https://doi.org/10.1002/2016GC006325, 2016.

Ezat, M. M., Rasmussen, T. L., Hönisch, B., Groeneveld, J., and deMenocal, P.: Episodic release of CO_2 from the high-latitude North Atlantic Ocean during the last 135 kyr, Nature Commun., 8, 14498, https://doi.org/10.1038/ncomms14498, 2017b.

Ezat, M. M., Rasmussen, T. L., Thornalley, D. J. R., Olsen, J., Skinner, L. C., Hönisch, B., and Groeneveld, J.: Ventilation history of Nordic Seas overflows during the last (de)glacial period revealed by species-specific benthic foraminiferal ^{14}C dates, Paleoceanography, 32, 172–181, https://doi.org/10.1002/2016PA003053, 2017a.

Ezat, M. M., Rasmussen, T. L., Skinner, L. C., and Zamelczyk, K.: Deep ocean ^{14}C ventilation age reconstructions from the Arctic Mediterranean reassessed, Earth Planet. Sci. Lett., 518, 67–75, https://doi.org/10.1016/j.epsl.2019.04.027, 2019.

Ezat, M. M., Rasmussen, T. L., Hain, M. P., Greaves, M., Rae, J. W. B., Zamelczyk, K., Marchitto, T. M., Szidat, S., and Skinner, L. C.: Deep Ocean Storage of Heat and CO_2 in the Fram Strait, Arctic Ocean During the Last Glacial Period, Paleoceanography, 36, https://doi.org/10.1029/2021PA004216, 2021.

Ezat, M. M., Fahl, K., Rasmussen, T.L.: Arctic freshwater outflow supressed Nordic Seas overturning and oceanic heat transport during the Last Interglacial, Nature Commun., 15, 8998, https://doi.org/10.1038/s41467-024-53401-3, 2024.

Fettweis, X., Box, J. E., Agosta, C., Amory, C., Kittel, C., Lang, C., van As, D., Machguth, H., and Gallée, H.: Reconstructions of the 1900–2015 Greenland ice sheet surface mass balance using the regional climate MAR model, Cryosphere, 11, 1015–1033, https://doi.org/10.5194/tc-11-1015-2017, 2017.

Fischer, H., Meissner, K.J., Mix, A.C., Abram, N.J., Austermann, J., Brovkin, V., Capron, E., Colombaroli, D., Daniau, A.L., Dyez, K.A., Felis, T., Finkelstein, S.A., Jaccard, S.L., McClymont, E.L., Rovere, A., Sutter, J., Wolff, E.W., Affolter, S., Bakker, P., Ballesteros-Cánovas, J.A., Barbante, C., Caley, T., Carlson, A.E., Churakova, O., Cortese, G., Cumming, B.F., Davis, B.A.S., De Vernal, A., Emile-Geay, J., Fritz, S.C., Gierz, P., Gottschalk, J., Holloway, M.D., Joos, F., Kucera, M., Loutre, M.F., Lunt, D.J., Marcisz, K., Marlon, J.R., Martinez, P., Masson-Delmotte, V., Nehrbass-Ahles, C., Otto-Bliesner, B.L., Raible, C.C., Risebrobakken, B., Sánchez Goñi, M.F., Arrigo, J.S., Sarnthein, M., Sjolte, J., Stocker, T.F., Velasquez Alvárez, P.A., Tinner, W., Valdes, P.J., Vogel, H., Wanner, H., Yan, Q., Yu, Z., Ziegler, M., Zhou, L.:

Palaeoclimate constraints on the impact of 2°C anthropogenic warming and beyond, Nat. Geosci, 11, 474–485, doi: 10.1038/s41561-018-0146-0, 2018.

Galaasen, E. V., Ninnemann, U. S., Irvalı, N., Kleiven, H. K. F., Rosenthal, Y., Kissel, C., and Hodell, D. A.: Rapid reductions in North Atlantic Deep Water during the peak of the last interglacial period, Science, 343, 1129–1132, 2014.Gottschalk, J., Skinner, L. C., Misra, S., Waelbroeck, C., Menviel, L., and Timmermann, A.: Abrupt changes in the southern extent of North Atlantic Deep Water during Dansgaard–Oeschger events, Nat. Geosci, 8, 950–954, https://doi.org/10.1038/NGEO2558, 2015.

Gottschalk, J., Battaglia, G., Fischer, H., Frölicher, T., Jaccard, S.L., Jeltsch-Thömmes, A., Joos, F., Köhler, P., Meissner, K.J., Menviel, L., Nehrbass-Ahles, C., Schmitt, J., Schmittner, A., Skinner, L.C., and Stocker, T.F.: Mechanisms of millennial-scale atmospheric CO_2 change in numerical model simulations, Quaternary Sci. Rev, 220, 30–74, https://doi: 10.1016/j.quascirev.2019.05.013, 2019.

Grant, K. M., Rohling, E. J., Bar-Matthews, M., Ayalon, A., Medina-Elizalde, M., Ramsey, C. B., Satow, C., and Roberts, A. P.: Rapid coupling between ice volume and polar temperature over the past 150,000 years, Nature, 491, 744–747, https://doi.org/10.1038/nature11593, 2012.

Groen, M. and Storey, M.: An astronomically calibrated $^{40}Ar/^{39}Ar$ age for the North Atlantic Z2 Ash: Implications for the Greenland ice core timescale, Quaternary Sci. Rev, 293, 107526, https://doi.org/10.1016/j.quascirev.2022.107526, 2022.

Guarino, M.-V., Sime, L. C., Schröeder, D., Malmierca-Vallet, I., Rosenblum, E., Ringer, M., Ridley, J., Feltham, D., Bitz, C., Steig, E. J., Wolff, E., Stroeve, J., and Sellar, A.: Sea-ice-free Arctic during the Last Interglacial supports fast future loss, Nat. Clim. Change, 10, 928–932, https://doi.org/10.1038/s41558-020-0865-2, 2020.

Guillevic, M., Bazin, L., Landais, A., Stowasser, C., Masson-Delmotte, V., Blunier, T., Eynaud, F., Falourd, S., Michel, E., Minster, B., Popp, T., Prié, F., and Vinther, B. M.: Evidence for a three-phase sequence during Heinrich Stadial 4 using a multiproxy approach based on Greenland ice core records, Clim. Past, 10, 2115–2133, https://doi.org/10.5194/cp-10-2115-2014, 2014.

Hathorne, E., Gagnon, A., Felis, T., Adkins, J., Asami, R., Boer, W., Caillon, N., Case, D., Cobb, K. M., Douville, E., deMenocal, P., Eisenhauer, A., Garbe-Schönberg, D., Geibert, W., Goldstein, S., Hughen, K., Inoue, M., Kawahata, H., Kölling, M., Cornec, F. L., Linsley, B. K., McGregor, H. V., Montagna,P., Nurhati, I. S., Quinn, T. M., Raddatz, J., Rebaubier, H., Robinso, L., Sadekov, A., Sherrell, R., Sinclair, D., Tudhope, A. W., Wei, G., Wong, H., Wu, H. C., and You, C.-F.: Interlaboratory study for coral Sr/Ca and other element/Ca ratio measurements, Geochem. Geophy. Geosy., 14, 3730–3750, https://doi.org/10.1002/ggge.20230, 2013.

Helmke, J.P. and Bauch, H.A.: Glacial–interglacial carbonate preservation records in the Nordic Seas, Global Planet. Change, 33, 15–28, https://doi.org/10.1016/S0921-8181(02)00058-9, 2002.

Hemming, S. R.: Heinrich events: Massive late Pleistocene detritus layers of the North Atlantic and their global climate imprint, Rev. Geophys., 42, https://doi.org/10.1029/2003RG000128, 2004.

Henrich, R.: Dynamics of Atlantic water advection to the Norwegian-Greenland Sea - a time-slice record of carbonate distribution in the last 300 ky, Mar. Geol., 145, 95–131, https://doi.org/10.1016/S0025-3227(97)00103-5, 1998.

Henrich, R., Heinz Baumann, K-H., Huber, R., Meggers, H.: Carbonate preservation records of the past 3 Myr in the Norwegian–Greenland Sea and the northern North Atlantic: implications for the history of NADW production, Mar. Geol., 184, 17–39, https://doi.org/10.1016/S0025-3227(01)00279-1, 2002.

Henry, L. G., McManus, J. F., Curry, W. B., Roberts, N. L., Piotrowski, A. M., and Keigwin, L. D.: North Atlantic ocean circulation and abrupt climate change during the last glaciation, Science, 353, 470–474, https://doi.org/10.1126/science.aaf5529, 2016.

Hermann, M., Papritz, L., and Wernli, H.: A Lagrangian analysis of the dynamical and thermodynamic drivers of large-scale Greenland melt events during 1979–2017, Weather Clim. Dynam., 1, 497–518, https://doi.org/10.5194/wcd-1-497-2020, 2020.

Hillaire-Marcel, C., Vernal, A. de, Bilodeau, G., and Weaver, A. J.: Absence of deep-water formation in the Labrador Sea during the last interglacial period, Nature, 410, 1073–1077, https://doi.org/10.1038/35074059, 2001.

Hoffmann, S. S., McManus, J. F., Curry, W. B., and Brown-Leger, L. S.: Persistent export of ^{231}Pa from the deep central Arctic Ocean over the past 35,000 years, Nature, 497, 603–606, https://doi.org/10.1038/nature12145, 2013.

Howe, J. N. W., Piotrowski, A. M., Noble, T. L., Mulitza, S., Chiessi, C. M., and Bayon, G.: North Atlantic Deep Water Production during the Last Glacial Maximum, Nat. Commun., 7, 11765, https://doi.org/10.1038/ncomms11765, 2016.

Inoue, M., Nohara, M., Okai, T., Suzuki, A., and Kawahata, H.: Concentrations of Trace Elements in Carbonate Reference Materials Coral JCp-1 and Giant Clam JCt-1 by Inductively Coupled Plasma-Mass Spectrometry, Geostand. Geoanal. Res., 28, 411–416, https://doi.org/10.1111/j.1751-908X.2004.tb00759.x, 2004.

Johns, W. E., Baringer, M. O., Beal, L. M., Cunningham, S. A., Kanzow, T., Bryden, H. L., Hirschi, J. J. M., Marotzke, J., Meinen, C. S., Shaw, B., and Curry, R.: Continuous, Array-Based Estimates of Atlantic Ocean Heat Transport at 26.5°N, J. Climate, 24, 2429–2449, https://doi.org/10.1175/2010JCLI3997.1, 2011.

Kandiano, E. S. and Bauch, H. A.: Implications of planktic foraminiferal size fractions for the glacial-interglacial paleoceanography of the polar North Atlantic, J. Foramin. Res., 32, 245–251, https://doi.org/10.2113/32.3.245, 2002.

Keigwin, L. D. and Swift, S. A.: Carbon isotope evidence for a northern source of deep water in the glacial western North Atlantic, P. Natl. ACAD. Sci. USA, 114, 2831–2835, https://doi.org/10.1073/pnas.1614693114, 2017.Kirby, N., Bailey, I., Lang, D.C., Brombacher, A., Chalk, T.B., Parker, R.L., Crocker, A.J., Taylor, V.E., Milton, J.A., Foster, G.L., Raymo, M. E., Kroon, D., Bell, D. B., and Wilson, P. A.: On climate and abyssal circulation in the Atlantic Ocean during late Pliocene marine isotope stage M2, ∼3.3 million years ago, Quaternary Sci. Rev., 250, 106644, https://doi.org/10.1016/j.quascirev.2020.106644, 2020.

Kleinen, T., Osborn, T.J. and Briffa, K.R.: Sensitivity of climate response to variations in freshwater hosing location, Ocean Dynam., 59, 509–521, https://doi.org/10.1007/s10236-009-0189-2, 2009.

Knies, J., Köseoğlu, D., Rise, L., Baeten, N., Bellec, V. K., Bøe, R., Klug, M., Panieri, G., Jernas, P. E., and Belt, S. T.: Nordic Seas polynyas and their role in preconditioning marine productivity during the Last Glacial Maximum, Nat. Commun., 9, 3959, https://doi.org/10.1038/s41467-018-06252-8, 2018.

Lacerra, M., Lund, D., Yu, J., and Schmittner, A.: Carbon storage in the mid-depth Atlantic during millennial-scale climate events, Paleoceanography, 32, 780–795, https://doi.org/10.1002/2016PA003081, 2017.

Lacerra, M., Lund, D., Gebbie, G., Oppo, D. W., Yu, J., Schmittner, A., and Umling, N. E.: Less remineralized carbon in the intermediate-depth South Atlantic during Heinrich Stadial 1, Paleoceanography, 34, 1218-1233, https://doi.org/10.1029/2018PA003537, 2019.

Larkin, C. S., Ezat, M. M., Roberts, N. L., Bauch, H. A., Spielhagen, R. F., Noormets, R., Polyak, L., Moreton, S. G., Rasmussen, T. L., Sarnthein, M., Tipper, E. T., and Piotrowski, A. M.: Active Nordic Seas deep-water formation during the last glacial maximum, Nat. Geosci., 15, 925–931, https://doi.org/10.1038/s41561-022-01050-w, 2022.

Lauvset, S. K., Lange, N., Tanhua, T., Bittig, H. C., Olsen, A., Kozyr, A., Alin, S., Álvarez, M., Azetsu-Scott, K., Barbero, L., Becker, S., Brown, P. J., Carter, B. R., Da Cunha, L. C., Feely, R. A., Hoppema, M., Humphreys, M. P., Ishii, M., Jeansson, E., Jiang, L.-Q., Jones, S. D., Lo Monaco, C., Murata, A., Müller, J. D., Pérez, F. F., Pfeil, B., Schirnick, C., Steinfeldt, R., Suzuki, T., Tilbrook, B., Ulfsbo, A., Velo, A., Woosley, R. J., and Key, R. M.: GLODAPv2.2022: the latest version of the global interior ocean biogeochemical data product, Earth Syst. Sci. Data, 14, 5543–5572, https://doi.org/10.5194/essd-14-5543-2022, 2022.

Lisiecki, L. E. and Raymo, M. E.: A Pliocene-Pleistocene stack of 57 globally distributed benthic $\delta^{18}O$ records, Paleoceanography, 20, https://doi.org/10.1029/2004PA001071, 2005.

Lisiecki, L. E. and Stern, J. V.: Regional and global benthic $\delta^{18}O$ stacks for the last glacial cycle, Paleoceanography, 31, 1368–1394, https://doi.org/10.1002/2016PA003002, 2016.

Locarnini, R. A., Mishonov, A. V., Baranova, O. K., Boyer T. P., Zweng, M. M., Garcia, H. E., Reagan, J. R., Seidov, D., Weathers, K., Paver, C. R., and Smolyar, I.: World Ocean Atlas 2018, Volume 1: Temperature: All years annual, 52 pp., 2018.

Lynch-Stieglitz, J., Stocker, T. F., Broecker, W. S., and Fairbanks, R. G.: The influence of air-sea exchange on the isotopic composition of oceanic carbon: Observations and modeling, Global Biogeochem. Cy., 9, 653–665, https://doi.org/10.1029/95GB02574, 1995.

Lynch-Stieglitz, J., Adkins, J. F., Curry, W. B., Dokken, T., Hall, I. R., Herguera, J. C., Hirschi, J. J.-M., Ivanova, E. V., Kissel, C., Marchal, O., Marchitto, T. M., McCave, I. N., McManus, J. F., Mulitza, S., Ninnemann, U., Peeters, F., Yu, E.-F., and Zahn, R.: Atlantic meridional overturning circulation during the Last Glacial Maximum, Science, 316, 66–69, https://doi.org/10.1126/science.1137127, 2007.

Marshall, J. and Schott, F.: Open-ocean convection: Observations, theory, and models, Rev. Geophys., 37, 1–64, https://doi.org/10.1029/98RG02739, 1999.

Mauritzen, C.: Production of dense overflow waters feeding the North Atlantic across the Greenland-Scotland Ridge. Part 1: Evidence for a revised circulation scheme, Deep Sea Research Part I: Oceanographic Research Papers, 43, 769–806, https://doi.org/10.1016/0967-0637(96)00037-4, 1996.

Mauritzen, C., Hansen, E., Andersson, M., Berx, B., Beszczynska-Möller, A., Burud, I., Christensen, K. H., Debernard, J., Steur, L. de, Dodd, P., Gerland, S., Godøy, Ø., Hansen, B., Hudson, S., Høydalsvik, F., Ingvaldsen, R., Isachsen, P. E., Kasajima, Y., Koszalka, I., Kovacs, K. M., Køltzow, M., LaCasce, J., Lee, C. M., Lavergne, T., Lydersen, C., Nicolaus, M., Nilsen, F., Nøst, O. A., Orvik, K. A., Reigstad, M., Schyberg, H., Seuthe, L., Skagseth, Ø., Skarðhamar, J., Skogseth, R., Sperrevik, A., Svensen, C., Søiland, H., Teigen, S. H., Tverberg, V., and Wexels Riser, C.: Closing the loop – Approaches to monitoring the state of the Arctic Mediterranean during the International Polar Year 2007–2008, Prog. Oceanogr., 90, 62–89, https://doi.org/10.1016/j.pocean.2011.02.010, 2011.

McManus, J. F., Francois, R., Gherardi, J.-M., Keigwin, L. D., and Brown-Leger, S.: Collapse and rapid resumption of Atlantic meridional circulation linked to deglacial climate changes, Nature, 428, 834–837, https://doi.org/10.1038/nature02494, 2004.

Mehrbach, C., Culberso, C. H., Hawley, J. E., and Pytkowic: Measurement of apparent dissociation constants of carbonic-acid in seawater at atmospheric pressure, Limnol. Oceanogr., 18, 897–907, https://doi.org/10.4319/lo.1973.18.6.0897, 1973.

Millo, C., Sarnthein, M., Voelker, A. and Erlenkeuser, H.: Variability of the Denmark Strait overflow during the Last Glacial Maximum, Boreas, 35, 50–60, https://doi.org/10.1111/j.1502-3885.2006.tb01112.x, 2006.

Misra, S., Greaves, M., Owen, R., Kerr, J., Elmore, A. C., and Elderfield, H.: Determination of B/Ca of natural carbonates by HR-ICP-MS, Geochem. Geophy. Geosy., 15, 1617–1628, https://doi.org/10.1002/2013GC005049, 2014.

Mortensen, A. K., Bigler, M., Grönvold, K., Steffensen, J. P., and Johnsen, S. J.: Volcanic ash layers from the Last Glacial Termination in the NGRIP ice core, J. Quaternary Sci., 20, 209–219, https://doi.org/10.1002/jqs.908, 2005.

Muglia, J. and Schmittner, A.: Carbon isotope constraints on glacial Atlantic meridional overturning: Strength vs depth, Quaternary Sci. Rev., 257, 106844, https://doi.org/10.1016/j.quascirev.2021.106844, 2021.

Nave, S., Lebreiro, S., Michel, E., Kissel, C., Figueiredo, M. O., Guihou, A., Ferreira, A., Labeyrie, L., and Alberto, A.: The Atlantic Meridional Overturning Circulation as productivity regulator of the North Atlantic Subtropical Gyre, Quaternary Res., 91, 399–413, https://doi.org/10.1017/qua.2018.88, 2019.

NGRIP Members: High-resolution record of Northern Hemisphere climate extending into the last interglacial period, Nature, 431, 147–151, https://doi.org/10.1038/nature02805, 2004.

Nørgaard-Pedersen, N., Spielhagen, R. F., Erlenkeuser, H., Grootes, P. M., Heinemeier, J., and Knies, J.: Arctic Ocean during the Last Glacial Maximum: Atlantic and polar domains of surface water mass distribution and ice cover, Paleoceanography, 18, https://doi.org/10.1029/2002PA000781, 2003.

Olafsson, J., Olafsdottir, S. R., Takahashi, T., Danielsen, M., and Arnarson, T. S.: Enhancement of the North Atlantic CO_2 sink by Arctic Waters, Biogeosciences, 18, 1689–1701, https://doi.org/10.5194/bg-18-1689-2021, 2021.

Olsen, A., Omar, A. M., Jeansson, E., Anderson, L. G., and Bellerby, R. G. J.: Nordic seas transit time distributions and anthropogenic CO_2, J. Geophys. Res., 115, https://doi.org/10.1029/2009JC005488, 2010.

Oppo, D. W., Gebbie, G., Huang, K.-F., Curry, W. B., Marchitto, T. M., and Pietro, K. R.: Data Constraints on Glacial Atlantic Water Mass Geometry and Properties, Paleoceanography, 33, 1013–1034, https://doi.org/10.1029/2018PA003408, 2018.

Oppo, D. W., Lu, W., Huang, K.-F., Umling, N. E., Guo, W., Yu, J., Curry, W. B., Marchitto, T. M., and Wang, S.: Deglacial Temperature and Carbonate Saturation State Variability in the Tropical Atlantic at Antarctic Intermediate Water Depths, Paleoceanography, 38, e2023PA004674, https://doi.org/10.1029/2023PA004674, 2023.

Østerhus, S., Woodgate, R., Valdimarsson, H., Turrell, B., Steur, L. de, Quadfasel, D., Olsen, S. M., Moritz, M., Lee, C. M., Larsen, K. M. H., Jónsson, S., Johnson, C., Jochumsen, K., Hansen, B., Curry, B., Cunningham, S., and Berx, B.: Arctic Mediterranean exchanges: a consistent volume budget and trends in transports from two decades of observations, Ocean Sci., 15, 379–399, https://doi.org/10.5194/os-15-379-2019, 2019.

Otto-Bliesner, B. L., Marshall, S. J., Overpeck, J. T., Miller, G. H., and Hu, A.: Simulating Arctic climate warmth and icefield retreat in the last interglaciation, Science, 311, 1751–1753, https://doi.org/10.1126/science.1120808, 2006.

Past Interglacials Working Group of PAGES: Interglacials of the last 800,000 years, Rev. Geophys., 54, 162–219, https://doi.org/10.1002/2015rg000482, 2016.

Paillet, J., Arhan, M., and McCartney, M. S.: Spreading of Labrador Sea Water in the eastern North Atlantic, J. Geophys. Res., 103, 10223–10239, https://doi.org/10.1029/98JC00262, 1998.

Pierrot, D. E., Wallace, D., and Lewis, E.: MS Excel program developed for CO_2 system calculations. Carbon Dioxide Information Analysis Center, 2011.

Pöppelmeier, F., Gutjahr, M., Blaser, P., Schulz, H., Süfke, F., and Lippold, J.: Stable Atlantic Deep Water Mass Sourcing on Glacial-Interglacial Timescales, Geophys. Res. Lett., 48, https://doi.org/10.1029/2021GL092722, 2021.

Quadfasel, D. and Meincke, J.: Note on the thermal structure of the Greenland Sea gyres, Deep Sea Research Part A. Oceanographic Research Papers, 34, 1883–1888, https://doi.org/10.1016/0198-0149(87)90061-6, 1987.

Quadfasel, D. and Käse, R.: Present-day manifestation of the Nordic Seas Overflows, in: Ocean Circulation: Mechanisms and Impacts—Past and Future Changes of Meridional Overturning, edited by: Schmittner, A., Chiang, J. C. H., and Hemming, S. R., American Geophysical Union, Washington, D. C., 75–89, https://doi.org/10.1029/173GM07, 2007.

Rahmstorf, S.: Ocean circulation and climate during the past 120,000 years, Nature, 419, 207–214, https://doi.org/10.1038/nature01090, 2002.

Railsback, L. B., Gibbard, P. L., Head, M. J., Voarintsoa, N. R. G., and Toucanne, S.: An optimized scheme of lettered marine isotope substages for the last 1.0 million years, and the climatostratigraphic nature of isotope stages and substages, Quaternary Sci. Rev., 111, 94–106, https://doi.org/10.1016/j.quascirev.2015.01.012, 2015.

Raitzsch, M., Hathorne, E. C., Kuhnert, H., Groeneveld, J., and Bickert, T.: Modern and late Pleistocene B/Ca ratios of the benthic foraminifer *Planulina wuellerstorfi* determined with laser ablation ICP-MS, Geology, 39, 1039–1042, https://doi.org/10.1130/G32009.1, 2011.

Rasmussen, S. O., Andersen, K. K., Svensson, A. M., Steffensen, J. P., Vinther, B. M., Clausen, H. B., Siggaard-Andersen, M.-L., Johnsen, S. J., Larsen, L. B., Dahl-Jensen, D., Bigler, M., Röthlisberger, R., Fischer, H., Goto-Azuma, K., Hansson, M. E., and Ruth, U.: A new Greenland ice core chronology for the last glacial termination, J. Geophys. Res., 111, https://doi.org/10.1029/2005JD006079, 2006.

Rasmussen, T. L., Thomsen, E., Labeyrie, L., and van Weering, T. C. E.: Circulation changes in the Faeroe-Shetland Channel correlating with cold events during the last glacial period (58–10 ka), Geology, 24, 937, https://doi.org/10.1130/0091-7613(1996)024<0937:CCITFS>2.3.CO;2, 1996.

Rasmussen, T. L., Thomsen, E., Kuijpers, A., and Wastegård, S.: Late warming and early cooling of the sea surface in the Nordic seas during MIS 5e (Eemian Interglacial), Quat. Sci. Rev., 22, 809–821, https://doi.org/10.1016/S0277-3791(02)00254-8, 2003.

Rasmussen, T. L. and Thomsen, E.: Ventilation changes in intermediate water on millennial time scales in the SE Nordic seas, 65-14 kyr BP, Geophys. Res. Lett., 36, https://doi.org/10.1029/2008GL036563, 2009.

Roach, A. T., Aagaard, K., and Carsey, F.: Coupled ice-ocean variability in the Greenland Sea, Atmos. Ocean, 31, 319–337, https://doi.org/10.1080/07055900.1993.9649474, 1993.

Rodrigues, T., Alonso-García, M., Hodell, D. A., Rufino, M., Naughton, F., Grimalt, J. O., Voelker, A., and Abrantes, F.: A 1-Ma record of sea surface temperature and extreme cooling events in the North Atlantic: A perspective from the Iberian Margin, Quaternary Sci. Rev., 172, 118–130, https://doi.org/10.1016/j.quascirev.2017.07.004, 2017.

Rysgaard, S., Bendtsen, J., Pedersen, L. T., Ramløv, H., and Glud, R. N.: Increased CO_2 uptake due to sea ice growth and decay in the Nordic Seas, J. Geophys. Res., 114, https://doi.org/10.1029/2008JC005088, 2009.

Sabine, C. L., Feely, R. A., Gruber, N., Key, R. M., Lee, K., Bullister, J. L., Wanninkhof, R., Wong, C. S., Wallace, D. W. R., Tilbrook, B., Millero, F. J., Peng, T.-H., Kozyr, A., Ono, T., and Rios, A. F.: The oceanic sink for anthropogenic CO_2, Science, 305, 367–371, https://doi.org/10.1126/science.1097403, 2004.

Sarnthein, M., Winn, K., Jung, S. J. A., Duplessy, J.-C., Labeyrie, L., Erlenkeuser, H., and Ganssen, G.: Changes in East Atlantic Deepwater Circulation over the last 30,000 years: Eight time slice reconstructions, Paleoceanography, 9, 209–267, https://doi.org/10.1029/93PA03301, 1994.

Schäfer, P., Thiede, J., Gerlach, S., Graf, G., Suess, E., and Zeitzschel, B.: The Environment of the Northern North-Atlantic Ocean: Modern Depositional Processes and their Historical Documentation, in: The Northern North Atlantic, edited by: Schäfer, P., Ritzrau, W., Schlüter, M., and Thiede, J., Springer Berlin Heidelberg, Berlin, Heidelberg, 1–17, https://doi.org/10.1007/978-3-642-56876-3_1, 2001.

Schlitzer, R.: Ocean Data View, https://doi.org/10013/epic.07f8e9e9-6111-47e9-a6dd-494af6f01c7b, 2022.

Schott, F., Visbeck, M., and Fischer, J.: Observations of vertical currents and convection in the central Greenland Sea during the winter of 1988–1989, J. Geophys. Res., 98, 14401, https://doi.org/10.1029/93JC00658, 1993.

Shackleton, N. J.: Attainment of isotopic equilibrium between ocean water and the benthonic foraminifera genus Uvigerina: Isotopic changes in the ocean during the last glacial, Colloques Internationaux Du C.N.R.S. - Les Méthodes Quantitatives d'etude Des Variations Du Climat Au Cours Du Pleistocene., 203–209, 1974.

Stobbe, T. B., Bauch, H. A., Frick, D. A., Yu, J., Gottschalk, J.: Bottom-water carbonate ion concentrations, oxygen and carbon isotopes, and pteropod abundances from Norwegian Sea sediment core PS1243 over the last 130,000 years. PANGAEA (last accessed: 21.01.2025), https://doi.org/10.1594/PANGAEA.973144

Sulpis, O., Agrawal, P., Wolthers, M., Munhoven, G., Walker, M., and Middelburg, J.J.: Aragonite dissolution protects calcite at the seafloor, Nature Commun., 13, 1104, https://doi.org/10.1038/s41467-022-28711-z, 2022.

Swift, J. H. and Aagaard, K.: Seasonal transitions and water mass formation in the Iceland and Greenland seas, Deep Sea Research Part A. Oceanographic Research Papers, 28, 1107–1129, https://doi.org/10.1016/0198-0149(81)90050-9, 1981.

Swift, J. H. and Koltermann, K. P.: The origin of Norwegian Sea Deep Water, J. Geophys. Res., 93, 3563–3569, https://doi.org/10.1029/JC093iC04p03563, 1988.

Tanhua, T., Olsson, K. A., and Jeansson, E.: Formation of Denmark Strait overflow water and its hydro-chemical composition, J. Marine Syst., 57, 264–288, https://doi.org/10.1016/j.jmarsys.2005.05.003, 2005.

Teal, L. R., Bulling, M. T., Parker, E. R., and Solan, M.: Global patterns of bioturbation intensity and mixed depth of marine soft sediments, Aquat. Biol., 2, 207–218, 2008.

Thibodeau, B., Bauch, H. A., and Pedersen, T. F.: Stratification-induced variations in nutrient utilization in the Polar North Atlantic during past interglacials, Earth Planet. Sc. Lett., 457, 127–135, 2017

Thornalley, D. J. R., Bauch, H. A., Gebbie, G., Guo, W., Ziegler, M., Bernasconi, S. M., Barker, S., Skinner, L. C., and Yu, J.: A warm and poorly ventilated deep Arctic Mediterranean during the last glacial period, Science, 349, 706–710, https://doi.org/10.1126/science.aaa9554, 2015.

Timmermans, M.-L. and Marshall, J.: Understanding Arctic Ocean Circulation: A Review of Ocean Dynamics in a Changing Climate, J. Geophys. Res. Oceans, 125, https://doi.org/10.1029/2018JC014378, 2020.

Trauth, M. H.: TURBO2: A MATLAB simulation to study the effects of bioturbation on paleoceanographic time series, Comput. Geosci., 61, 1–10, https://doi.org/10.1016/j.cageo.2013.05.003, 2013.

Uppström, L. R.: The boron/chlorinity ratio of deep-sea water from the Pacific Ocean, Deep Sea Research and Oceanographic Abstracts, 21, 161–162, https://doi.org/10.1016/0011-7471(74)90074-6, 1974.

Vázquez-Rodríguez, M., Touratier, F., Lo Monaco, C., Waugh, D. W., Padin, X. A., Bellerby, R. G. J., Goyet, C., Metzl, N., Ríos, A. F., and Pérez, F. F.: Anthropogenic carbon distributions in the Atlantic Ocean: data-based estimates from the Arctic to the Antarctic, Biogeosciences, 6, 439–451, https://doi.org/10.5194/bg-6-439-2009, 2009.

Veres, D., Bazin, L., Landais, A., Toyé Mahamadou Kele, H., Lemieux-Dudon, B., Parrenin, F., Martinerie, P., Blayo, E., Blunier, T., Capron, E., Chappellaz, J., Rasmussen, S. O., Severi, M., Svensson, A., Vinther, B., and Wolff, E. W.: The

Antarctic ice core chronology (AICC2012): an optimized multi-parameter and multi-site dating approach for the last 120 thousand years, Clim. Past, 9, 1733–1748, https://doi.org/10.5194/cp-9-1733-2013, 2013.

Veum, T., Jansen, E., Arnold, M., Beyer, I., and Duplessy, J.-C.: Water mass exchange between the North Atlantic and the Norwegian Sea during the past 28,000 years, Nature, 356, 783–785, https://doi.org/10.1038/356783a0, 1992.

Watson, A. J., Schuster, U., Bakker, D. C. E., Bates, N. R., Corbière, A., González-Dávila, M., Friedrich, T., Hauck, J., Heinze, C., Johannessen, T., Körtzinger, A., Metzl, N., Olafsson, J., Olsen, A., Oschlies, A., Padin, X. A., Pfeil, B., Santana-Casiano, J. M., Steinhoff, T., Telszewski, M., Rios, A. F., Wallace, D. W. R., and Wanninkhof, R.: Tracking the variable North Atlantic sink for atmospheric CO_2, Science, 326, 1391–1393, https://doi.org/10.1126/science.1177394, 2009.

Weinelt, M., Sarnthein, M., Pflaumann, U., Schulz, H., Jung, S. and Erlenkeuser, H.: Ice-free Nordic seas during the last glacial maximum? Potential sites of deepwater formation, Paleoclimates, 1, 283–309, 1996.

Winsor, K., Carlson, A. E., Klinkhammer, G. P., Stoner, J. S., and Hatfield, R. G.: Evolution of the northeast Labrador Sea during the last interglaciation, Geochem. Geophy. Geosy., 13, https://doi.org/10.1029/2012GC004263, 2012.

Yu, J. and Elderfield, H.: Benthic foraminiferal B/Ca ratios reflect deep water carbonate saturation state, Earth Planet. Sc. Lett., 258, 73–86, https://doi.org/10.1016/j.epsl.2007.03.025, 2007.

Yu, J., Elderfield, H., Greaves, M., and Day, J.: Preferential dissolution of benthic foraminiferal calcite during laboratory reductive cleaning, Geochem. Geophy. Geosy., 8, https://doi.org/10.1029/2006GC001571, 2007.

Yu, J., Elderfield, H., and Piotrowski, A. M.: Seawater carbonate ion-$\delta^{13}C$ systematics and application to glacial–interglacial North Atlantic Ocean circulation, Earth Planet. Sc. Lett., 271, 209–220, https://doi.org/10.1016/j.epsl.2008.04.010, 2008.

Yu, J., Foster, G. L., Elderfield, H., Broecker, W. S., and Clark, E.: An evaluation of benthic foraminiferal B/Ca and $\delta^{11}B$ for deep ocean carbonate ion and pH reconstructions, Earth Planet. Sc. Lett, 293, 114–120, https://doi.org/10.1016/j.epsl.2010.02.029, 2010a.

Yu, J., Broecker, W.S., Elderfield, H., Jin, Z., McManus, J., Zhang, F..: Loss of carbon from the deep sea since the Last Glacial Maximum. Science 330, 1084–1087, https://doi.org/10.1126/science.1193221, 2010b.

Yu, J., Anderson, R. F., Jin, Z., Menviel, L., Zhang, F., Ryerson, F. J., and Rohling, E. J.: Deep South Atlantic carbonate chemistry and increased interocean deep water exchange during last deglaciation, Quaternary Sci. Rev., 90, 80–89, https://doi.org/10.1016/j.quascirev.2014.02.018, 2014.

Yu, J., Menviel, L., Jin, Z. D., Thornalley, D. J. R., Barker, S., Marino, G., Rohling, E. J., Cai, Y., Zhang, F., Wang, X., Dai, Y., Chen, P., and Broecker, W. S.: Sequestration of carbon in the deep Atlantic during the last glaciation, Nat. Geosci, 9, 319–324, https://doi.org/10.1038/NGEO2657, 2016.

Yu, J., Menviel, L., Jin, Z. D., Thornalley, D. J. R., Foster, G. L., Rohling, E. J., McCave, I. N., McManus, J. F., Dai, Y., Ren, H., He, F., Zhang, F., Chen, P. J., and Roberts, A. P.: More efficient North Atlantic carbon pump during the Last Glacial Maximum, Nat. Commun., 10, 2170, https://doi.org/10.1038/s41467-019-10028-z, 2019.

Yu, J., Menviel, L., Jin, Z. D., Anderson, R. F., Jian, Z., Piotrowski, A. M., Ma, X., Rohling, E.J., Zhang, F., Marino, G., and McManus, J.F.: Last glacial atmospheric CO_2 decline due to widespread Pacific deep-water expansion. Nat. Geosci, 13, 628–633, https://doi.org/10.1038/s41561-020-0610-5, 2020.

Yu, J., Anderson, R. F., Jin, Z. D., Ji, X., Thornalley, D. J. R., Wu, L., Thouveny, N., Cai, Y., Tan, L., Zhang, F., Menviel, L., Tian, J., Xie, X., Rohling, E. J., and McManus, J. F.: Millennial atmospheric CO_2 changes linked to ocean ventilation modes over past 150,000 years, Nat. Geosci, 16, 1166–1173, https://doi.org/10.1038/s41561-023-01297-x, 2023.

Zweng, M. M., Reagan, J. R., Seidov, D., Boyer, T. P., Locarnini, R. A., García, H. E., Mishonov, A. V., Baranova, O. K., Weathers, K., Paver, C. R., and Smolyar, I.: World Ocean Atlas 2018: Volume 2: Salinity. A. Mishonov Technical Ed; NOAA Atlas NESDIS 82, 50 pp., 2018.